Efficient economic optimisation of large-scale tidal stream arrays

Z. L. Goss[1], D. S. Coles[2], S. C. Kramer[1], and M. D. Piggott[1]

[1]Department of Earth Science and Engineering, Imperial College London, SW7 2AZ, UK
[2]School of Engineering, Computing and Mathematics, University of Plymouth, Plymouth PL4 8AA, UK

March 31, 2022

Abstract

As the tidal energy industry moves from demonstrator arrays comprising just a few turbines to large-scale arrays made up of potentially hundreds of turbines, there is a need to optimise both the number of turbines and their spatial distribution in order to minimise cost of energy. Optimising array design manually may be feasible for small arrays, but becomes an impractically large approach when the number of devices is high, especially if taking into account both the cost effectiveness of each turbine and also the coupled nature of the turbine locations and the local as well as far-field hydrodynamics.

Previous work has largely focused on producing computational tools to automatically design the size and layout of large-scale tidal turbine arrays to optimise power. There has been some limited preliminary work to incorporate costs into these models, in order to improve the economic viability of tidal arrays. This paper provides the first in depth implementation and analysis of economic functionals, based upon metrics such as break even power and levelised cost of energy, used for design of explicit array sizing and spatial variation.

The addition of these new economic functionals introduces complexity by increasing the number of inputs to the model, each of which are subject to their own uncertainty in value. For this reason, sensitivity analysis becomes both more important as well as more difficult to undertake. This paper presents a novel rapid methodology for deriving the optimal array design (number of turbines and their spatial distribution throughout the farm area) to minimise cost functionals, and its sensitivity to variations in the economic inputs. Importantly, the new aspects of this method introduced here do not rely on repeated model runs and iterative optimisation, two aspects that typically prove to be impractically expensive computationally. This more readily allows for the impact of changes in investor priorities to be investigated. It is also shown that, while the optimal solution varies greatly with uncertainty in the input parameters, this uncertainty is reduced significantly through Monte Carlo analysis.

1 Introduction

In recent years the price of offshore wind has fallen dramatically, with record-low prices of £39.65/MWh seen in the UK's third Contracts for Difference auction [1]. Currently, tidal stream and other ocean energies must compete against offshore wind for subsidies and other forms of government support, however tidal stream is at a much earlier stage of development. As a result of this, tidal energy is currently a higher cost technology and needs further development pathways to remove this barrier to market penetration [2]. Commercial-scale tidal stream energy arrays have yet to be deployed, and so the emerging industry needs to rely on models to help understand the factors affecting array performance, including coupled interactions to the hydrodynamics. Laboratory experiments have practical limitations and have only tested limited configurations, e.g. comprising two to ten three-bladed rotors, notably by Stallard et al. [3] and Mycek et al. [4], so computational models must be relied on as the number of turbines in an array increases. This motivates the need for innovative tools, which can be used to optimise the array design to reduce the cost of tidal energy [5, 6, 7, 8, 9].

As the tidal energy industry develops, cost reductions are anticipated to come in many forms, some from improved technological solutions such as cheaper or easier to install foundations or higher rated rotors [10]. In order to achieve commercial viability in an open market, reductions in the cost of energy must also come through improved array design using existing technology. Many tools have been created which can predict and maximise the yield of tidal stream arrays. Optimal array design can take advantage of the economies of volume that result from larger scale arrays and can lead to higher yields from intelligent micro-siting of the turbines to minimise negative blockage effects. For example [6] found that the yield of an optimised array layout in an open channel increased by up to 38%, compared to a regular grid layout, and that in a strait between an island and a landmass the yield increased by 22%. Similarly, [5] demonstrated optimisation of layout within a square basin and found the power production of 152 turbines in a regular non-staggered grid layout increased by 104% from 41.4MW to 84.5MW when using an irregular optimised layout.

More recently, hydrodynamic models of potential tidal array sites have been implemented in *Thetis* — coastal ocean modelling software which allows the array design to be coupled with the flow and enables gradient-based optimisation through the availability of an adjoint mode [5, 6, 11, 12]. Earlier iterations of these tools focused on optimising with respect to power alone [7, 8, 13]. However, modelling array power alone does not take into account the diminishing returns in yield per device as the number of turbines in an array increases. This decrease in the average power per device is due to both blockage effects and turbine spacing requirements which lead to additional turbines being placed in lower flow areas. Therefore there is a need to incorporate the balance of costs associated with adding turbines to an array against the additional yield gained from them, to decide on both an optimal number of turbines and suitable locations.

Later adaptations of these tools incorporated costs by introducing a break even power, P_{BE}, to the optimisation functional, such that there is an effective capacity factor that turbines must achieve in order to be cost efficient to install [14, 15]. Introducing a break even power into the functional is a simple way to bring the balance of maximising power vs minimising costs into the optimisation of array design. However, this approach relies on a lot of assumptions, and does not account for many factors which may make one array design more advantageous over another. For example, in the form used in previous work, break even power is assumed to be independent of the number of turbines. In practice there may be economies of volume, such that the effective costs of turbines, and therefore P_{BE}, decreases as the number of turbines increases. This paper provides a new understanding of how economies of volume impacts upon optimal array design by applying a factor to decrease the break even power with the number of turbines. Choosing an appropriate value for this factor and the break even power itself relies on a complex balance of metrics not explicitly included, such as the lifetime of array, discounted cash flow analysis and the balance of CAPEX and OPEX.

This paper furthers these investigations into break even powers, by using more holistic economic indicators as the optimisation functional. It advances on previous array optimisation studies, through a novel approach to explicit array sizing and spatial distribution with respect to a realistic model for profitability. There are a number of different ways to express the profitability of a tidal stream array, including the Net Present Value (NPV), Internal Rate of Return (IRR), Return on Investment (ROI), Payback Period (PP) and Levelised Cost of Energy (LCOE). All of these metrics take into account the sum of energy generated over an array's lifetime, and the sum of costs incurred over the lifetime. These metrics each have different advantages and times when they may be more appropriate to use. Policy makers often use LCOE as a simple metric to enable like-for-like comparisons of the performance of different energy technologies. This is the most common metric used by institutions such as the Offshore Renewable Energy Catapult (OREC), the Centre for Climate Finance & Investment (CCFI) and Green Investment Bank (GIB) [16, 17, 18], and thus is investigated in Section 6.3.

More holistic economic indicators bring in many more parameters for a better representation of true array financing, however this large parameter space also adds uncertainty. It becomes intractable to perform optimisations over all possible sets of costs inputs. To overcome this problem, this paper describes the development of a new emulator approach which enables rapid testing of the functional over a large range of parameters. The construction of the novel emulator method is based on the realisation that despite the many forms the economic models and their associated functional(s), they can typically be reduced to a bi-objective trade-off between number of turbines and realisable power output with the optimal result for any given functional being Pareto efficient. The emulator is then combined with Monte Carlo based sensitivity analysis to allow for better

understanding of the uncertainty by defining a P10 to P90 confidence interval.

Section 2 describes the inputs for the financial models and the ways that costs of tidal energy may fall. Section 3 presents the model for break even power and LCOE. Section 4 gives the details of the idealised model used as a simple representation of a typical tidal site. Section 5 shows the results of optimising a farm within this simple channel, over different break even powers. Section 6 describes how the results from optimising over a range of break even powers can be used to build an emulator for the rapid evaluation of the LCOE (or other economic models) over many different combinations of cost inputs. Section 6.1 outlines the process that can be used to apply the developed emulator method to real-world array design. An application of the methodology developed in this paper appears in [19], showing that it can be used to predict the LCOE that can be achieved in the Alderney Race for different levels of deployment. This shows that the methods developed and validated in this paper can be applied for assessment of the economic viability of real-world tidal sites.

2 Inputs and cost reduction pathways

The Offshore Renewable Energy Catapult (OREC) describe a number of potential mechanisms for cost reduction in the tidal stream energy sector [16]. The three main categories for cost reduction described are economies of scale, economies of volume and learning rates. It is important to be aware of the distinction between the different types of cost reduction, since some of them can be exploited through optimal location and numbers of turbines and others cannot. For clarity, economies of scale will refer to the cost reductions that can be achieved by moving towards higher rated power or larger rotor devices. Economies of volume will refer to the cost reductions achievable from higher numbers of turbines in arrays, such as benefits of mass-manufacturing (as per the convention set by OREC).

Learning rates refer to how the costs fall due to learning by doing. This can include; optimised installation and maintenance processes learnt through repeated operations, technology innovations learnt from previously installed arrays or even other forms of offshore energy, and improved commercial terms due to previously installed arrays providing proof of concept, reducing the perceived risk to investors. This paper will distinguish between learning cost reductions versus economies of volume, as costs falling due to an increase in installed cumulative capacity versus costs falling due to increased number of turbines within one array [20].

Previous work [21] identified a range of cost parameter estimates, by reviewing publicly available information on tidal energy costs. There is a wide range in values for each cost parameter, in part because very few tidal-stream turbines or arrays have been installed at the time of writing and in part because cost information is commercially sensitive. The review calculated a pessimistic, typical and optimistic value for each parameter, shown in Table 1.

In this study only economies of volume will be explicitly investigated. Economies of volume are implemented through the distinction between fixed and turbine-dependent costs in Table 1. Turbine-dependent costs, CA_t and O_t, are the costs that increase linearly with the number of turbines, such as the price of the turbines themselves or the inter-array cabling. Fixed costs, CA_f and O_f, are the costs that are independent of the number of turbines, such as site assessments and any costs charged at a flat rate. As the number of turbines is increased these fixed costs are split over more devices, and therefore the costs per MW falls due to economies of volume. The use of these different cost components to mimic the cost curves found in literature is described in greater detail in [21].

Economies of scale cannot be considered because it is assumed that at the start of the design optimisation process that the size and rating of the turbines is specified. This is necessary because the optimisation method used accounts for the coupled effect of the array design and the hydrodynamics, and therefore the size and rating must be known so that the power and drag can be calculated from the appropriate power and thrust curves.

Learning rates will be subject to the cumulative installed capacity, and developers will have no influence over this at the point of designing an array. Furthermore it is hard to predict the extent to which technology innovation and decreased cost of capital can be achieved. While not explicitly calculated in this work, the three scenarios in Table 1 are investigated and it is likely that learning rates will be the mechanism by which costs within the industry fall from the pessimistic and typical range towards the optimistic scenarios.

All economic models used in this paper are evaluated using a typical year, where the revenue is assumed to be constant year-on-year and is a product of

$$Rev_i = P_{\text{avg}} \times t_i \times T_e, \tag{1}$$

where P_{avg} is the time averaged power in MW, which is assumed to be constant each year, t_i is the number of hours generating in year i and T_e is the electricity tariff in £/MWh.

The MeyGen project reports a project-wide availability of 95% [22]. However, this assumption was made before the array was operational and it was anticipated that the turbines would exceed their target performance in practice. Due to the lack of publicly available and validated estimates, this paper assumes 100% availability, so $t_i = 365 \times 24$ hours, however the model user can replace this with their own, potentially commercially sensitive values in practice. The electricity tariff, T_e, is likely to remain constant because in its early stages tidal energy will rely on fixed-price subsidies such as Contracts for Difference (CfDs). However, the power generation is time varying and even if yield is averaged on a yearly basis it will fluctuate due to the 18.6 year lunar nodal cycle [23, 24]. The number of generating hours will also vary because the number of faults and need for maintenance will likely increase as the devices age, as has been seen in the offshore wind industry [25, 26]. This study assumes a constant value of generating hours to reflect the 'average' year because when demonstrating the methods on an idealised test case, the year the array goes into production is not known. Also at the time of writing, tidal arrays have not yet been in production long enough to build an accurate model of the anticipated increase in downtime with time.

The presence of turbines in the flow can have unintended negative environmental and ecological impacts on the surrounding area. Neil et al. demonstrated that commercial-scale arrays in the vicinity of a headland could have significant impact on nearby sandbanks through disrupting the sediment transport [27]. Studies by du Feu et al. [8, 13] demonstrate how environmental impact can be incorporated into an array optimisation functional through the addition of a penalty term to the array profit. This approach could easily be combined with the revenue given in Equation 1 to optimise the trade-off between economic performance and environmental impact, but this paper focuses on economics alone.

The sum of all array expenditure incurred in year i, Ex_i, is assumed to be split into Capital Expenditures (CAPEX) incurred in year zero and Operational Expenditures (OPEX) incurred every year after installation, such that $i \in [1, L]$ where L is the lifetime of the array. Vazquez et al. [28] estimated that the CAPEX for a tidal stream array typically break down into 41% device costs, 26% foundations costs, 15% installation costs, 13% cable costs and 5% grid connection costs. This is comparable to the CAPEX breakdown reported by MeyGen, except the foundations accounted for only 11% [29]. OPEX is primarily comprised of maintenance costs (with planned and unplanned accounting for 15% and 21% of the MeyGen annual OPEX budget respectively [29]). Lease and insurance costs (32%) and spare parts (14%) make up 46% of the OPEX outlay. Similarly to power generation, OPEX is assumed to be constant each year in this model, however in practice it could be adjusted to increase with time, assuming failure rate increases. Development costs are not included in this work because access to data is limited and these costs are expected to be a relatively low proportion of costs in comparison to CAPEX and OPEX. A more detailed review of tidal costs and the methods used to obtain the estimates in Table 1 is given in [21].

Typically CAPEX and OPEX are modelled as a cost per MW installed, which falls as the number of turbines in an array increases [30, 31]. [21] demonstrated how this is equivalent to assuming that each expenditure type linearly increases with the number of turbines. The CAPEX can therefore be written as

$$\text{Ex}_{i=0} = \text{CAPEX} = \text{CA}_f + \text{CA}_t \times n_t \tag{2}$$

and similarly the OPEX is estimated by

$$\text{Ex}_{i>0} = \text{OPEX} = \text{O}_f + \text{O}_t \times n_t, \tag{3}$$

where n_t is the number of turbines and CA_f, CA_t, O_f and O_t are the fixed and turbine-dependent components of CAPEX and OPEX, estimates for which are summarised in Table 1. The use of this linear relationship helps to model economies of volume. In real arrays the relationship is not likely to be exactly linear but it is a good approximation and can be used to demonstrate the effectiveness of the following array optimisation methods. If used in practice tidal developers could easily replace these cost assumptions with their own internal financial models.

2.1 Turbine specifications

The cost inputs in Table 1 are all from calculations made in [21], which are calculated using the assumption that the turbines are 16m in diameter and 2MW rated power. This is based on the amount of cost information available for different turbine sizes, and an average of the most common turbine specifications [32, 20, 10, 33].

The turbines are assumed to have a thrust coefficient below rated of $C_T = 0.8$ [34] and a power coefficient below rated of $C_P = 0.41$ [20]. Again this is based on commonly found values in the literature, however all these parameters could be readily updated in order to optimise an array of turbines with different specifications.

3 Economics modelling methods

In the following section the increasingly detailed methods used to bring economic considerations into the array optimisation process are discussed. Initially break even power is added as a proxy for the costs of the turbines, then the break even power is adapted to account for economies of volume. Finally a model of the Levelised Cost of Energy (LCOE) of the array is implemented as the functional instead. Each model makes a number of assumptions, outlined below.

3.1 Break even power

The break even power is the average power over all turbines that needs to be generated in order for the array to break even over its lifetime, such that

$$\sum_{i=0}^{L} P_{\mathrm{BE}} \times T_e \times t_i \times n_t - \mathrm{Ex}_i = 0, \tag{4}$$

where P_{BE} is the break even power in MW, T_e is the electricity tariff, i.e. the price per MWh the electricity generated is sold at, i is the year the costs are being evaluated over, L is lifetime of the array in years, t_i is the number of hours generating in year i and Ex_i is the sum of all array expenditure incurred in year i. The concept is discussed in more detail in [21].

For the array to generate a profit the average total power generated by the array must be more than the average break even power per device, multiplied by the total number of devices. It is therefore simple to include these economic considerations into the optimisation functional of interest, J, such that

$$\max_{P,n_t} J(P, n_t) = P - P_{\mathrm{BE}} \times n_t. \tag{5}$$

If an appropriate P_{BE} is chosen to reflect all of the costs that comprise Ex_i in Equation (4), this choice of functional effectively maximises the profit and penalises the addition of turbines which do not generate enough power to outweigh their costs.

Section 5.1 demonstrates the impact of varying the break even power from $P_{\mathrm{BE}} = 0$, such that the functional optimises power alone, increasing to find the maximal value of P_{BE}, such that the turbines become so expensive that the optimal array design contains no turbines.

3.1.1 Break even power with economies of volume

The functional shown in Equation 5, would result in a design with the optimal number of turbines if the break even power were constant over arrays of all sizes. However, in practice economies of volume would result in a lower P_{BE} required to break even for large-scale arrays than for small scale arrays. This is discussed in greater detail in [21]. For simplicity this paper investigates a P_{BE} that linearly decreases with the number of turbines, at a rate of EV. EV is varied through 0.00005, 0.0001, 0.00015 and 0.0002 MW. For example, if an array of 2MW turbines has a P_{BE} of 0.8MW, the minimum required capacity factor for one turbine to be economically viable is 40% (=0.8MW/2MW). However, with an EV of 0.0001MW and an array with 100 turbines would have a reduced the break even power of 0.6MW (=0.8MW-100×0.0001MW) the capacity factor would need to be just 30% (=0.6MW/2MW). This results in the following functional

$$\max_{P,n_t} J(P, n_t) = P_{\mathrm{avg}} - (P_{\mathrm{BE}} - EV \times n_t) \times n_t = P_{\mathrm{avg}} - P_{\mathrm{BE}} \times n_t + EV \times n_t^2, \tag{6}$$

where P_{BE} and EV are the break even power and economies of scale to be specified in the functional, J, and P and n_t are the power and number of turbines in the array design being optimised.

Section 5.2 investigates how adding different extents of economies of volume to the break even power impacts upon optimal array design.

3.2 LCOE

A more robust way to include economies of volume in the functional is to calculate the levelised cost of energy (LCOE). The LCOE is a proxy for the average price of energy, T_e [£/MWh], that an array must receive in order to break even over its lifetime. The LCOE allows all of the costs to be summed up, in this case based on the assumed relationship between number of turbines from Equations 2 and 3. It also uses discounted cash flow analysis, such that a discount rate, r, is applied annually to account for the decreasing time value of money to investors. It can therefore be calculated from

$$\mathrm{LCOE} = \frac{\text{discounted cost}}{\text{discounted energy}} = \frac{\sum_{i=0}^{L} \frac{\mathrm{Ex}_i}{(1+r)^i}}{\sum_{i=0}^{L} \frac{E_i}{(1+r)^i}}. \tag{7}$$

where Ex_i is the sum of all array expenditure incurred in year i, E_i is the energy generated by the array in year i, and L is the lifetime of the array in years.

If using the approximation to CAPEX and OPEX found in Equations 2 and 3, this can be used as a functional to optimise, such that

$$\min_{P,n_t} J(P,n_t) = \mathrm{LCOE} = \frac{\mathrm{CA}_f + \mathrm{CA}_t \times n_t + \sum_{i=1}^{L} \frac{O_f + O_t \times n_t}{(1+r)^i}}{\sum_{i=1}^{L} \frac{E_i}{(1+r)^i}}. \tag{8}$$

CA_f, CA_t, O_f and O_t are the fixed and turbine-dependent components of CAPEX and OPEX, which are defined in Equations 2 and 3 with typical estimates for their values summarised in Table 1. A full comparison of LCOE to other metrics such as Net Present Value, Internal Rate of Return and Payback Period is given in [21].

4 Idealised model set-up

In this work, the above economic optimisation methods are applied to an idealised channel set-up. Draper et al. [35] characterised coastal sites that are especially suitable for tidal stream energy extraction due to accelerated flow via four generic coastline configurations. These sites are a strait between two infinite ocean basins, a headland, an enclosed bay, and a strait between an island and a semi-infinite landmass.

Many tidal energy resource studies focus on the Alderney Race as a potential site, due to it's highly concentrated energy potential [36]. SIMEC Atlantis and the Development Agency for Normandy have a joint venture plan to install up to 2GW of tidal capacity in the Race. Much like the generic idealised site of flow between an island and a semi-infinite landmass, the flow is accelerated as it is confined between the Isle of Alderney and Cap de la Hague in France. The velocities can reach up to $5\,\mathrm{m\,s^{-1}}$, resulting in an estimated maximum average power potential of 5.1 GW [37]. Since the Alderney Race is most similar to Draper et al.'s final idealised case, this study focuses on the optimisation of a tidal arrays within the strait between an island and a landmass. Peréz-Ortiz et al. [38] recently investigated power extraction by narrow arrays (similar to tidal fences) spanning across such a strait. This work extends upon that by optimising array design and studying large-scale arrays rather than tidal fences, so there is more freedom in where the turbines can be placed. The following sections describe the setup of this idealised model. UK wide resource assessments have identified that 'first generation' tidal-stream sites require peak spring tidal velocities in excess of $2.5\,\mathrm{m\,s^{-1}}$ and depths between 25 and 50 m [39, 40]. Both the Alderney Race and this idealised setup satisfy those conditions.

4.1 Numerical model in *Thetis*

A flexible finite-element based coastal ocean model, *Thetis*, is used to solve the shallow water equations on an unstructured triangular mesh [12]. *Thetis* is built using the *Firedrake* framework

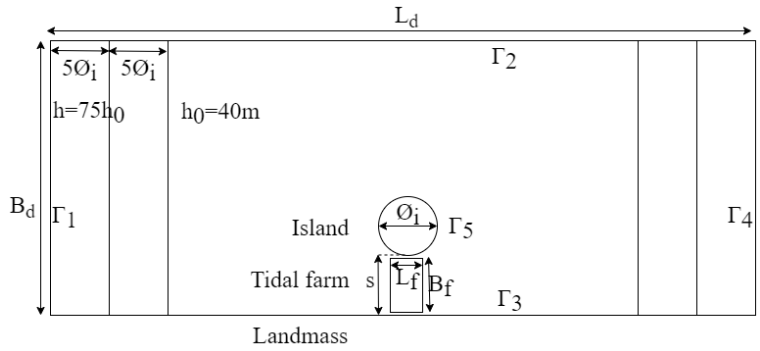

Figure 1: Idealised geometry for a model of flow through a channel with an island of diameter $\emptyset_i = 2\,\text{km}$ and a tidal site of area $A_f = B_f \times L_f$ where turbines can be added. The depth is increased linearly from h_0 to $75h_0$ to mimic the conditions at the continental shelf. $L_d = 140\,\text{km}$ is the length of the channel and $B_d = 40\,\text{km}$ is the width. $s = 2\,\text{km}$ is the minimum distance from the island to the southern landmass. This matches the setup used used in [14] (not to scale).

(https://www.firedrakeproject.org/), which automates the generation of optimised low level application code from high level descriptions of finite element discretisations specified using the domain-specific Unified Form Language (UFL) [41]. *Thetis* is the coastal ocean modelling package chosen for use here since it is open-source and the adjoint mode allows the array design process to be coupled with the hydrodynamic model [5, 6, 11, 12], enabling optimisation of the functionals defined in Equations 5, 6 and 8.

Flow through the channel is modelled here using the nonlinear shallow water equations which are considered here, in the non-conservative form:

$$\begin{aligned} \frac{\partial \eta}{\partial t} + \nabla \times (H\mathbf{u}) &= 0, \\ \frac{\partial \mathbf{u}}{\partial t} + \mathbf{u}\cdot\nabla\mathbf{u} - \nu\nabla^2\mathbf{u} + g\nabla\eta + C_d\frac{|\mathbf{u}|\mathbf{u}}{H} &= 0, \end{aligned} \tag{9}$$

where η is the free surface perturbation, t is time, H is the total water depth (the sum of η and the still water depth), $\mathbf{u} = (u, v)$ is the 2D depth-averaged velocity vector, ν is the kinematic viscosity of the fluid which here is set to a value of $10^{-4}\,\text{m}^2\,\text{s}^{-1}$, g is acceleration due to gravity, and C_d is a dimensionless quadratic drag coefficient for seabed friction, set to 0.0025. Due to simplifying assumptions Coriolis, wind and wave conditions, and atmospheric pressure are not included in this work.

4.2 Simplified model parameterisation

The geometry of the channel and the island is adapted from [38], and uses the same values as their setup where the channel in this domain is is $L_d = 140\,\text{km}$ long and $B_d = 40\,\text{km}$ wide, with a circular island of diameter $\emptyset_i = 2\,\text{km}$ located in the middle of the channel. It has a minimum distance from the island to the southern landmass of $s = 2\,\text{km}$. This is shown is Fig. 1.

The farm area, A_f, is $L_f = 1\,\text{km}$ long and $B_f = 1.92\,\text{km}$ wide, as shown Fig. 2. This is to approximately represent the dimensions of the Alderney Race tidal lease plots available to build on, spanning across about half of the length of the island and the whole width of the strait, with a 0.4 km buffer to the edge of the southern land mass and the island. In the region between 20 km and 10 km from from the eastern and western boundaries, the water depth is linearly increased in the streamwise direction from $h_0 = 40\,\text{m}$, which is the depth throughout the majority of the domain, to $75h_0$ in the band within 10km of the boundaries. This depth profile, shown alongside the computational mesh in Fig. 2, was chosen by [38] to mimic the conditions at the edge of the continental shelf and help prevent spurious reflections at the boundary.

4.3 Tidal forcing and boundaries

The domain shown in Fig. 1 has solid boundaries which correspond to a semi-infinite landmass, at the northern and southern sides of the domain, Γ_2 & Γ_3, on which a free slip boundary condition

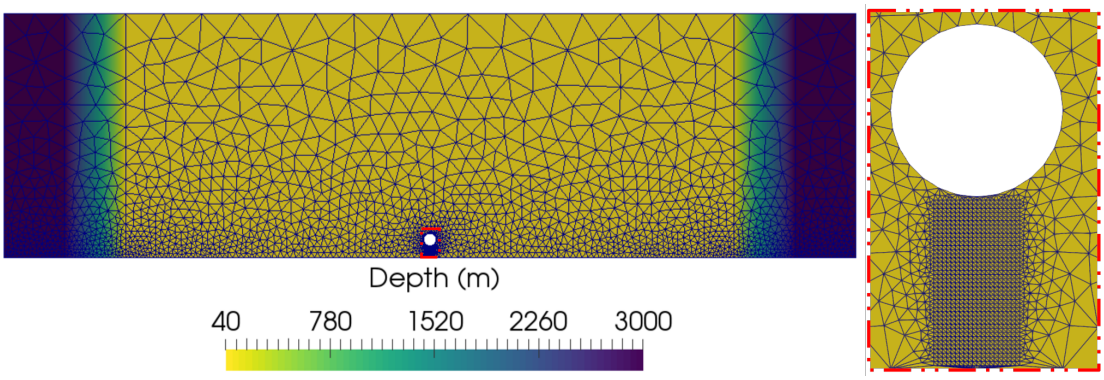

Figure 2: Multi-scale triangular computational mesh across the idealised domain. This is overlaid on a map of depths which increase from 40m to 3000m at the open boundaries. An enlarged view of the regular isosceles triangular mesh used within the farm area is shown on the right. This domain and mesh are identical to those used in [15] and are adapted from the setup used in [38].

is applied. A free slip boundary condition is also applied to the solid boundary of the circular island, Γ_5. There are open boundaries on the western and eastern side of the channel, Γ_1 & Γ_4 respectively. Here M2 tidal forcing is applied to the free surface perturbation variable, which has an amplitude of $a = 3\,\mathrm{m}$ and a frequency of $\omega_t = 1.41 \times 10^{-4}\,\mathrm{rad\,s^{-1}}$, such that

$$\eta = a_0 a \sin(\omega_t t). \tag{10}$$

The multiplier $a_0 = 0.5(1 - \cos(\omega_t t/4))$ is used to ramp up the tidal signal over the first two tidal cycles. The model is run for seven tidal cycles in total, with the third and fourth being excluded to allow for spin up once the model has fully ramped up and time averages are only taken over the final three tidal cycles.

4.4 Discretisation of the model

Many discretisation options are available in *Thetis* due to the flexibility afforded by the use of the *Firedrake* mesh generation framework. In this work piecewise-linear, discontinuous basis functions are used to represent both the velocity and the free surface fields (the $\mathrm{P_{1DG}}-\mathrm{P_{1DG}}$ velocity-pressure finite element pair). The shallow water equations are solved on an unstructured triangular mesh, which is generated by defining the element edge length on each boundary region.

The element edge length used in the unstructured part of the mesh is coarsest on the northern landmass, Γ_2, to a value of $\pi\emptyset_i = 6.28km$. It is set finer along the southern landmass, Γ_3, at $\pi\emptyset_i/6 = 1.05km$ due to proximity to the array area. The finest resolution in the unstructured part of the mesh is specified around the island boundary, Γ_5, at a value of $\pi\emptyset_i/28 = 0.22km$. A regular grid of 20 by 40 right isosceles angled triangles is used in all meshes for the tidal farm area, corresponding to an edge length of 48m by 50m. This results in a mesh with 5010 elements overall. The boundaries, $\Gamma_1 : 5$, are specified in Fig. 1 and tidal farm area and resultant mesh are shown in Fig. 2. As far as the hydrodynamics are concerned, the numerical setup is identical to the model used in [15] and [14] and therefore the mesh convergence study used to decide on this mesh resolution is not repeated here.

For the temporal discretisation a Crank-Nicolson time stepping method is used, with $\Delta t = 800\,\mathrm{s}$. This was also chosen as an appropriate time step size in a previous study [15], through a time step independence test for Δt varying from 1600 s down to 100 s.

4.5 Turbine representation

This work uses a continuous approach for turbine representation, as proposed in [5], where a spatially varying turbine density field, $d(\mathbf{x})$, is optimised. This approach, which does not attempt to represent individual turbines rather their 'concentration', is suitable for coarser mesh resolutions. It optimises the total number of turbines and their location (in an averaged sense) together within one optimisation loop. This greatly reduces the computational cost, which is important for modelling large-scale arrays.

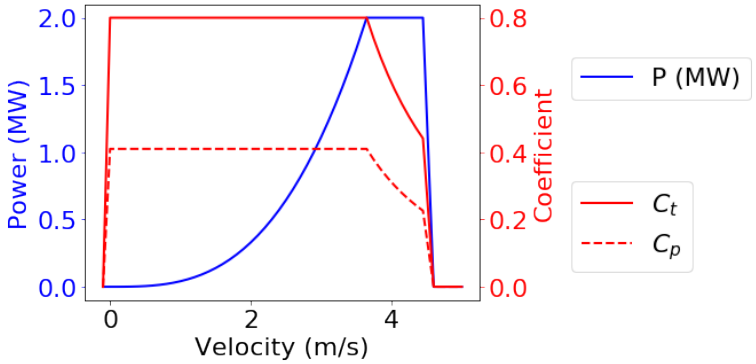

Figure 3: Power curve of a typical generic tidal turbine assumed for this work.

Turbines are only allowed to be placed within the predefined farm area, A_f, and are modelled through the inclusion of an additional bottom friction term of the form

$$\frac{c_t}{\rho H}||\mathbf{u}||\mathbf{u}, \tag{11}$$

which is added to the left hand side of the Shallow Water Equations (9). ρ is the water density. The bottom friction coefficient, c_t, can be found from the turbine density field $d(\mathbf{x})$ via

$$c_t(d(\mathbf{x})) = \frac{1}{2}C_T A_T d(\mathbf{x}), \tag{12}$$

where A_T is the swept area of the turbines, which in this study is based on the 16 m diameter 2 MW OpenHydro turbines or 1.5 MW turbines installed in the MeyGen project. The turbine density is given a maximum allowable upper limit which is chosen to represent a high but still plausible, upper bound density of turbines. It corresponds to a minimum inter-device spacing of 2.5 turbine diameters centre-to-centre laterally and 5 turbine diameters in the stream-wise direction, or equivalently a 1.25 diameter lateral spacing and 10 diameter downstream spacing. The turbines have a cut in speed of $1m/s$ and a cut out speed of $4.5m/s$. C_T, the turbine thrust coefficient, which corresponds to the idealised thrust curve shown in Fig. 3, is 0.8 below rated and is scaled by $\frac{u^3_{rated}}{u^3}$ above rated speed. In reality the drag force will be increased partly due to the rotor thrust represented in Equation (11) and in part due to the drag of the turbine structure system. The latter is not included explicitly in this work, because the drag of the structure is relatively small compared to the rotor thrust and this work considers a highly idealised example to demonstrate this new method of economic optimisation. Furthermore, the calculation of the support structure drag depends on design chosen by manufacturers, so this paper remains generalised by simply using a high C_T [42]. The implications of this assumption and a method for handling the turbine structure drag is discussed in Section 7.

The turbine density can be integrated over the array area to find the total number of turbines, n_t, such that

$$\int_{A_f} d(\mathbf{x})\, d\mathbf{x} = n_t. \tag{13}$$

The power is found similarly

$$P = \frac{1}{2}\rho A_T \int_{A_f} C_P\, d(\mathbf{x})\, ||\mathbf{u}||^3\, d\mathbf{x}, \tag{14}$$

and is then time averaged before use in the optimisation functional, to help quantify the financial success of the array. C_P, the turbine power coefficient, is 0.41 below rated [20] and is scaled by $\frac{u^3_{rated}}{u^3}$ above rated speed, as also show in in Fig. 3.

Experiments were carried out in [43], to investigate the validity of using a depth-averaged continuous drag method of representing turbines for tidal resource analysis. Porous fences spanning the width of a recirculating flume were used to simulate the added drag of a large, multi-row, uniformly-distributed array of tidal turbines. Load cells were used to measure the thrust force on each porous fence, and these measurements were compared to the results of the continuous drag

method. The level of agreement between the depth-averaged flow speeds used in Equation (11) and the local flow through the turbine rotor (represented by the porous fences) determines the accuracy of the depth-averaged continuous drag method for representing turbines. This agreement was shown to be dependent on the level of wake recovery and longitudinal spacing between rows and the magnitude of the ambient turbulence, which aids the mixing between the wakes and the accelerated bypass flow. Bed mounted ADCPs have shown that while the turbines are operational the turbulence intensity at the MeyGen 1A site is 10–12% [44]. Actuator disc experiments have found these turbulence intensities to correspond to an approximately 40% wake deficit at 5 diameters downstream and an approximately 20% deficit at 10 diameters downstream [45].

Further studies [46, 47, 48] demonstrate that wake impingement on downstream turbines in relatively dense arrays causes depth averaged flow speeds to overestimate the true flow speeds through the turbine rotor. The maximum array density has been specified to allow for sufficient longitudinal spacing between rows, to address this effect and allow for wake recovery. The European Marine Energy Centre (EMEC) recommend a greater spacing of 2.5 turbine diameters centre to centre and 10 diameter downstream, however they acknowledge that this can be shown to be a conservative spacing requirement once detailed wake effect modelling is undertaken [49]. The maximum allowable turbine density is therefore chosen to be slightly higher than this guideline, and to allow for designs with decreased lateral spacing between turbines. Numerical simulations in idealised channel flows by Consul et al. [50] showed that yield increases of up to 23% could be achieved by increasing blockage ratios and the recently developed Orbital O2 tidal device consists of two 1MW 20m diameter turbines mounted either side of a floating superstructure, with a 25m distance centre-to-centre. This is equivalent to a 1.25 diameter spacing laterally, so the upper limit on the turbine density used in this paper in that case would be equivalent to imposing a minimum spacing of 10 turbine diameters downstream. This work demonstrates the method of optimising arrays to minimise the LCOE on an idealised domain. When applying this method to modelling real tidal sites the limitations on the turbine spacing can be updated as relevant information becomes available for a given site. An appropriate upper limit on the turbine density for any given site can be chosen once site specific ambient turbulence has been characterised, since turbulence intensity and length scales relative to rotor diameter have been shown to have a significant impact on wake recovery rate [45].

4.6 Adjoint-based optimisation

Optimisation of the array design, with respect to the different economic functionals outlined above, is performed using $d(\mathbf{x})$ as the control parameter. The optimisation procedures begins with zero turbines everywhere, then on each iteration the forward model is run (solving the shallow water equations coupled with the turbine friction to find the power and other array characteristics, as described above), then the functional values are recalculated. The adjoint is calculated (via `http://pyadjoint.readthedocs.io/` library), to find the sensitivity of the functional to changes in the turbine density, while coupled to changes in the hydrodynamics. This information is fed into a L-BFGS-B based optimisation algorithm, to update the turbine density field in such a way so as to optimise the economic functional of choice. An optimal design is converged upon and the algorithm is completed, typically for this scenario within 5 to 20 iterations.

5 Array optimisation

An idealised set-up is used to test the impact of different functionals, which account for economic factors in increasing levels of detail, on optimal array design. First, the impact of varying break even power is investigated, followed by an optimisation where the break even power depends on the number of turbines employed through economies of volume. Similar studies that vary break even power [15] and economies of volume [14] are extended here over a greater range, to form the basis of the new optimisation procedure developed in the next section.

5.1 Varying break even power

The array design is optimised within the farm area, A_f, where the flow is accelerated in the vicinity of the island in the constricted channel setup shown in Fig. 1. Fig. 4 shows how the optimal array design varies as the break even power increases, using the functional described in Equation (5).

In Fig. 5 it is shown that as the break even power increases the net average power of the array and the number of turbines in the optimal array design decreases, because turbines are effectively more expensive to install, while the power per device increases, because fewer turbines result in lower blockage.

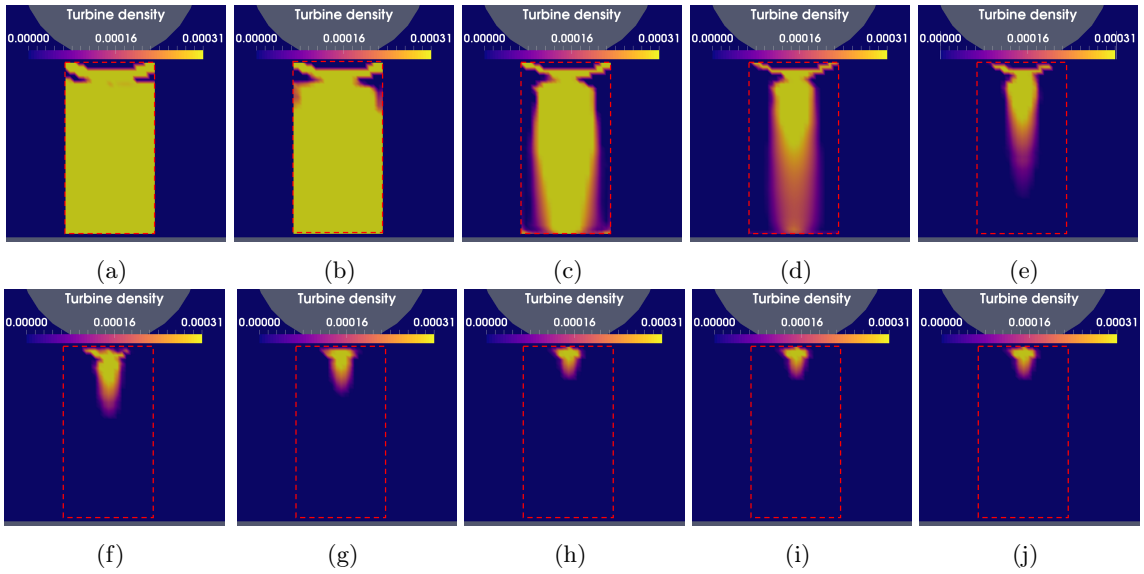

Figure 4: Array designs optimised for $J = P - P_{BE} \times n_t$, with a break even power of (a) 0, (b) 0.1, (c) 0.2, (d) 0.3, (e) 0.4, (f) 0.5, (g) 0.6, (h) 0.7, (i) 0.8 and (j) 0.9 MW. The farm boundary is shown in red, areas with maximum turbine density are shown in yellow and no turbines shown in blue.

The break even power is varied from P_{BE} = 0MW to 1.3MW. $1.3MW$ is the highest break even power that can be specified before the optimal design consists of no turbines because the flow is not high enough for any one turbine in any location within A_f to generate more than 1.3MW. The optimisation is also performed in the other extreme for P_{BE} = 0MW. While this is possible numerically, in reality the break even power would never be zero, because that would mean that the turbines are free. Setting the break even power to zero thus changes the functional from an economic one to one that optimises for power alone. This is commonly used in some array optimisation studies ([6, 51, 52]) and is sensible if there is already a fixed number of turbines chosen. However, having a non-zero and appropriately chosen break even power becomes crucial if the number of turbines varies, because this allows the right balance between maximising power and minimising costs to be found. Including this as a case has two benefits, firstly to demonstrate the limit of no economic penalty and investigate financial models over a broad range of sample points, even extreme ones.

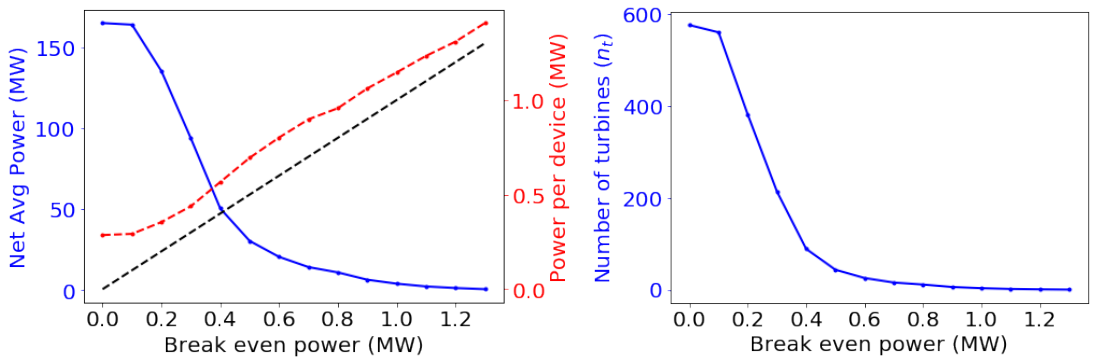

Figure 5: Variations in the total array power generated and the number of turbines for the optimal design as P_{BE} is increased, adapted from [15]. The black line shows that the average power per device (in red) always stays higher than the P_{BE} chosen in the functional.

Secondly it helps demonstrate the impact of global blockage. In Fig. 4a, even though there is no cost associated with the turbines because $P_{BE} = 0$MW, there are no turbines added in the semi-circular region around the island. Adding turbines here creates so much blockage that the power generated by the additional turbines is offset by the losses experienced by the other turbines. This array design represents a hypothetical maximum of how much power could be extracted if cost were not an issue, but in reality would never be economically practical.

A qualitative shift can be observed for $0.2 \leq P_{BE} \leq 0.4$MW, where the optimal array design paradigm shifts between a barrage or fence-like design that spans across the whole width of the channel (to exploit the benefits of channel-scale blockage control) to a cluster of turbines close to the island just taking advantage of the locally high flow velocities. This can be seen clearly though the sharp drop in net average power and optimal number of turbines, shown in Fig. 5. In this region small changes to the functional result in large changes to the optimal array design. This is problematic for array design, because there may be uncertainty in the appropriate choice of P_{BE} and it may vary with array size due to economies of volume. These results are discussed in more detail in [15].

5.2 Break even power with economies of volume : results

Next, realism is added to the functional, by making the break even power decrease linearly with number of turbines, such that $P_{\mathrm{BE}} \Rightarrow P_{\mathrm{BE}} - \mathrm{EV} \times n_t$, where EV is a parameter representing economies of volume. Fig. 6 shows how the macro array parameters, such as optimal number of turbines, total array power and average power per device, vary with the break even power and economies of volume.

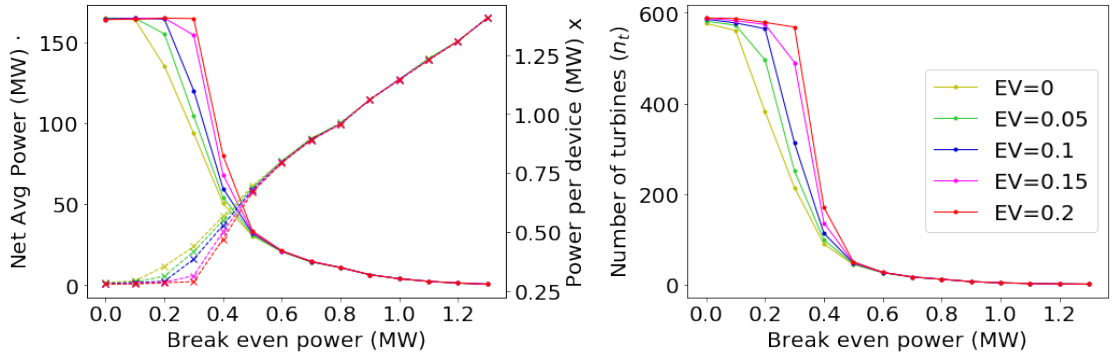

Figure 6: Variations in the average power generated and the number of turbines for the optimal design as P_{BE} and ev are increased.

Fig. 6 demonstrates that as the economies of volume are increased, the optimal number of turbines increase and therefore the total array power increases, since higher numbers of turbines result in lower costs per turbine. However, the power per device decreases, because through economies of volume the turbines are effectively cheaper and therefore do not need to generate as much power to be worth installing.

A key result of both of these pieces of work is that the optimal array design is greatly dependent on the choice of functional, and especially sensitive to small changes in the break even power for mid range values in the region $0.2 \leq P_{BE} \leq 0.4$. Changes to the scaling parameter EV, make relatively little impact on the optimal array design outside of this range and a significant impact within it. This shows that the optimal array design is very sensitive to changes in P_{BE} at mid-range values (for more details see [14]). Since both functionals used are a simplification of the true profitability of an array, there is a need to optimise for a more complete financial model.

6 Economic Emulator

Each of the optimisation scenarios presented in Section 5 are obtained through running the full hydrodynamic model in a computationally expensive optimisation loop. This paper presents an original method, where those optimisation runs can be performed in order to generate data to construct an emulator. The emulator can be used for the rapid assessment of optimal array

parameters (such as number of turbines, array power and power per device) over a large range of functionals. This emulator is demonstrated by optimising LCOE over a variety of cost inputs. In order to validate the emulator predictions of optimal LCOE and number of turbines, the LCOE formula defined in Equation (8) is used as the functional in a fully coupled hydrodynamic model and optimisation in *Thetis*. This is the first instance of coupling a hydrodynamic model of an array design in *Thetis* with a complex financial model of the array, such as LCOE, used as the functional of interest.

6.1 Schema of emulator-based methodology for the economic analysis of array design

The following sections present, in detail, the development and validation of an emulator method, which is demonstrated to be fast and flexible at identifying optimal array characteristics. The process developed can be applied to real world array design. A simplified summary of the steps to optimise a tidal array design in practice is as follows:

1. Build and validate a hydrodynamic model of the region of interest in *Thetis*.
2. Perform adjoint optimisation of the array design with respect to $J = P_{avg} - P_{BE} \times n_t$ over a range of sufficiently many (approximately ten to twenty here) different values of P_{BE}. This yields a set of turbine densities and corresponding optimal power versus number of turbines data points.
3. Interpolate between those data points to build an emulator to predict the optimal power that can be achieved over all possible numbers of turbines.
4. Use the emulator to feed P_{avg} and n_t values into an economic model of choosing, such as LCOE, Net Present Value, Internal Rate of Return or Payback Period. Choose the array size which optimises the metric of interest.
5. Perform Monte Carlo sensitivity analysis over the full range of uncertainty in the cost inputs used in the economic model, obtain P50, P10 and P90 values, which translate to the median value and 80% confidence interval.
6. Use this more detailed analysis to decide on an array size that keeps the P10, P50 and P90 predictions within a desirable range.
7. Perform a final full adjoint optimisation of the array size chosen to produce a map of the spatial distribution of turbines and validate the predictions of the emulator.

6.2 Building an emulator by finding the Pareto frontier

In Section 5.1 three parameters appear in the functional for break even power alone; P, n_t and P_{BE}, where in this work both P are n_t are found as a function of the turbine density field $d(\mathbf{x})$ and are obtained through the optimisation process. This is true for the extended scenario in Section 5.2 also, with the addition of a fourth parameter for economies of volume, EV. There are therefore one or two parameters (P_{BE} or P_{BE} and EV) in each of the previous sections, which need to be decided upon before running the optimisation, each of which has uncertainty involved in the choice of parameter value. When there are only one or two input parameters to vary it is relatively easy to investigate the impact of this uncertainty. The optimisation process can simply be run repeatedly so that the impact that changes in parameter values over their plausible range make on the optimal design can be investigated.

However, when optimising for LCOE or other economic models which are derived from Net Present Value (NPV) analysis there are a large number of uncertain input parameters. NPV calculations require not only P and n_t to be known, but also r, L, T_e and all of the costs across all of the years of the array's lifetime. In this work those costs are simplified to be represented by only four parameters, C_t, C_f, O_t and O_f, by the assumptions made in (2) and (3). Even with this simplification, this would still require varying the chosen input parameters within a seven dimensional space to test the impact of uncertainty. This reduces to six dimensional space when using LCOE models instead of NPV, by removing the need to specify T_e — the input with arguably the most uncertainty [21] — through optimising at the break even point, NPV = 0. Full uncertainty

quantification via the variation of all input parameters, would be prohibitively expensive because it would require an optimisation to be performed for every set of parameters.

This creates a need for a simpler, computationally cheaper proxy model, with which the uncertainty analysis can be performed through consideration of a great range of parameter values. In all of the economic models considered in this work, the costs are assumed independent of the turbine locations. Therefore, for the scenario considered here there will be an optimal array design which achieves maximal power for each possible number of turbines – from 0 to 576 (the number of turbines at which maximal power can be generated). With the maximum density, $d(\mathbf{x})$ and farm area, A_f, specified in Fig. 1, up to 600 turbines could be installed, but any more than 576 would generate less power than the optimal solution for $P_{BE} = 0$, from Fig. 4a. While there are no location-based costs, the optimisation procedure can be reduced to a bi-objective optimisation problem of choosing the optimal balance between number of turbines (corresponding to the costs of the array) and net average power (corresponding to the revenues of the array). Further work could include location-based costs at the site-scale by adjusting the CAPEX and OPEX appropriately for the average distance to shore and depth, using the spatial tool developed by Vazquez and Iglesias [28].

Therefore, the optimal power that can be achieved for a given number of turbines can be plotted against number of turbines, as shown in Fig. 7 (a). If a curve can be fitted between these points, each of which is found through the *Thetis* optimisation of the spatially-varying turbine density, then a bi-objective trade-off curve is found, where improving either the power or number of turbines deteriorates the other parameter. Any formulation of the functional, which monotonically increases with power for a fixed n_t and, reversely, monotonically decreases with n_t for a fixed power, will have an optimal solution which falls somewhere along this trade-off curve. In multi-objective optimisation, this is known as a Pareto frontier, where the points on the trade-off curve form the set of all Pareto efficient solutions. Pareto efficiency is a condition where no performance criterion can be improved upon without a trade-off making at least one other criterion worse. In this case, each optimal solution shown in Fig. 7 (a) is Pareto efficient because the power can not increase without the number of turbines (and therefore the cost) increasing, and vice versa. The different economic models and choice of input parameters values just shift the weighting between the two.

The values from the break even power study are just used as an example of how the Pareto frontier can be explored using a simple functional and by varying one parameter. Increasing P_{BE} from 0 to rated power ensures that there are samples distributed across the Pareto frontier. Once the sample points are obtained, for example from the break even power study, an emulator for the optimal achievable power for each number of turbines can be created, here through the use of quadratic (cubic giving essentially the same result) spline interpolation between each successive pair of points. Quadratic spline interpolation is sufficient to produce a smooth curve between the optimal points found from the break even power study and increasing to cubic spline interpolation had little impact on the shape of the curve fitted. This curve can be used to predict the optimal net power that can be achieved as a function of the number of turbines in an array, i.e. $P \equiv P(n_t)$. Therefore, the optimisation can be considered a problem in just one dimension – choosing the optimal number of turbines for the economic functional chosen.

Fig. 7 (a) demonstrates how this interpolation, for the fourteen data points obtained from optimisation runs when break even power varies from 0 to 0.8 MW, can be used to build an emulator to predict the net average array power and other related characteristics such as power per device. The emulator is used to produce the curve of predicted net powers, shown in blue, and predicted average powers per device, shown in red. The predictions generated by this emulator are compared in Fig. 7 (b) to the results obtained when optimising for break even power with economies of volume, based on the functional (6). This testing demonstrated that quadratic spline interpolation is more than sufficient to match the *Thetis* model data. It can be seen that running the computationally expensive *Thetis* optimisation model only fourteen times is enough to obtain good predictions for these 84 optimisation scenarios. A user may be able to reduce the number of optimisation model runs needed if some minimum array power level is required to make a significant energy contribution, which would allow the minimum number of turbines considered to be increased above the low numbers included in this example, for example.

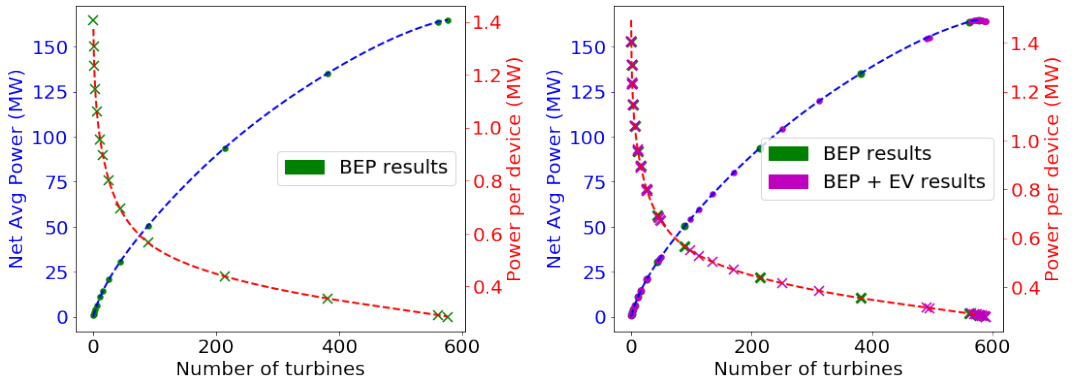

(a) (b)

Figure 7: (a) The fourteen data points from the break even power study (shown in green) and the emulator for optimal power that can be generated from these as a function of the number of turbines. (b) The emulator compared to the optimised array parameters from 36 simulations optimising for break even power with economies of volume added (shown in magenta). For both studies the optimised array power is marked by a dot and the optimised power per device is marked by a cross.

6.3 LCOE Results

Once the emulator has been generated, instead of re-running the expensive optimisation loop in *Thetis*, the LCOE can be estimated across all possible n_t values, with the corresponding $P(n_t)$ values found from the emulator. The n_t which minimises the LCOE can then be obtained. Fig. 8 shows this approach for finding the optimal LCOE and corresponding number of turbines for three different sets of parameter values. The first set uses the typical values shown in Table 1, the second set uses the highest L values and the lowest values for all other parameters in order to find the optimal LCOE in the best case scenario given the uncertainty in parameter values, and the final set uses the reverse to find the optimal LCOE in the worst case scenario.

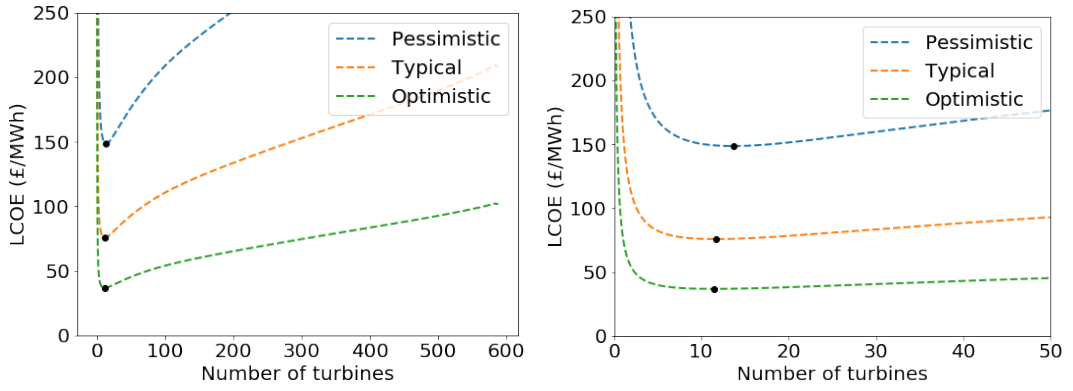

(a) (b)

Figure 8: The emulator prediction for LCOE across all n_t values from 0 to 600 and a snapshot around the optimal values. The optimal LCOE for each set of parameter values is shown as a black dot, and the input parameters are chosen to match the pessimistic, typical and optimistic values shown in Table 1.

Results presented in Appendix A demonstrate how the emulator can be used to enable the prediction of the optimal array design for LCOE under a large range of parameter values. The main findings are that the CAPEX has more influence on the LCOE and optimal array features than the OPEX, due to CAPEX accounting for a higher percentage of the lifetime costs, especially when a high discount rate is applied. The turbine-dependent components of the costs, CA_t and O_t, have more impact on the LCOE than the fixed components. This is despite the fixed components

having a greater uncertainty range to vary over (the pessimistic estimate for CA_f is 2.5 times the optimistic estimate, whereas the pessimistic estimate for CA_t is 1.8 times the optimistic estimate) and the fixed components being approximately three times the size of their respective turbine dependent components (CA_f is 2.3, 2.8 and 3.2 times the size of CA_t in the optimistic, typical and pessimistic cases respectively. Similarly O_f is 2.9, 2.1 and 3.3 times the size of O_t in the optimistic, typical and pessimistic cases). This is because the turbine dependent components of the costs are multiplied by the number of turbines, so becomes more dominant as the number of turbines increases. The results presented in Appendix A also demonstrate that when the cost parameter values change the LCOE varies a lot more than the optimal number of turbines. Overall it demonstrates that the variability of the optimal solution with different parameter choices is interconnected with other parameter choices. This is an example of in depth sensitivity analysis that would be computationally prohibitive to perform using direct optimisation over a vast number of different functionals.

6.3.1 Emulator validation for LCOE results

Fig. 9 shows how the number of turbines and LCOE for the final iterations of the *Thetis* optimisation procedure compare to the curve found using the emulator for the optimal LCOE that can be achieved for each number of turbines in the array. The optimal LCOE and corresponding number of turbines from the emulator is marked as a black dot, with the final iteration of the *Thetis* optimisation marked with a black cross. Three scenarios are compared – when all the parameters are set to their typical value from Table 1 and when all are set to their typical value except CA_t, which is set to the maximum and minimum value.

This comparison demonstrates how the selection of the optimal design differs between the two methods; the emulator starts by estimating the LCOE for the optimal design for each number of turbines, then selects the number of turbines that minimises this, the *Thetis* model starts with an initial turbine density field then optimises it until the LCOE improves no more. The final iterations are included in Fig. 9 to make the point that each iteration will always be on or above the curve from the emulators. This is because the *Thetis* model starts with a non-optimal turbine configuration and improves the density field until it ends up on the configuration that optimises the given functional, whereas the emulator starts with the Pareto frontier, where the turbine configuration maximises the power generation for any given number of turbines, and from this information selects the n_t which optimises the functional.

Fig. 10 compares the optimal solution obtained via the *Thetis* model to the predictions of the emulator. Since the emulator is much cheaper to run, predictions across the whole range of parameters from max to min are shown, whereas only the max, min and typical values are shown for the *Thetis* model. These results show that the predictions for LCOE are quite accurate and the emulator is suitable for predicting LCOE. However, they also show that the predictions for the optimal number of turbines has a much greater error. Inspection of Fig. 9 shows that the LCOE curves are relatively flat and very insensitive to changes in the number of turbines near to the optimal solution. This shows that the optimal solution may be a robust one, however accuracy in n_t predictions may be harder to obtain because of this. Furthermore the magnitude of the error is approximately one turbine or less, except for the optimistic CA_f scenario, where it is almost two turbines.

Fig. 11 shows how each of the solutions obtained via the *Thetis* model lie on (or very close to) the Pareto frontiers for optimal array power and power per device, obtained from the emulator. This further supports the conclusion that the emulator can be used to accurately find the set of array designs with an optimal trade-off between number of turbines and power.

6.3.2 Monte Carlo evaluation of LCOE predictions

Since there is a significant degree of uncertainty in the input parameters from Table 1, there is a drastic difference between the LCOE predictions in the optimistic and pessimistic scenarios shown in Fig. 8. This LCOE variation is so large partly due to the fact that the costs are commercially sensitive so it is hard to obtain an academic prediction of them. They are also subject to change with time, because costs in the industry will fall due to learning rates. However, variation is also exaggerated due to the pessimistic and optimistic scenarios being the combination of all inputs at their most extreme values, when in practice this is very unlikely.

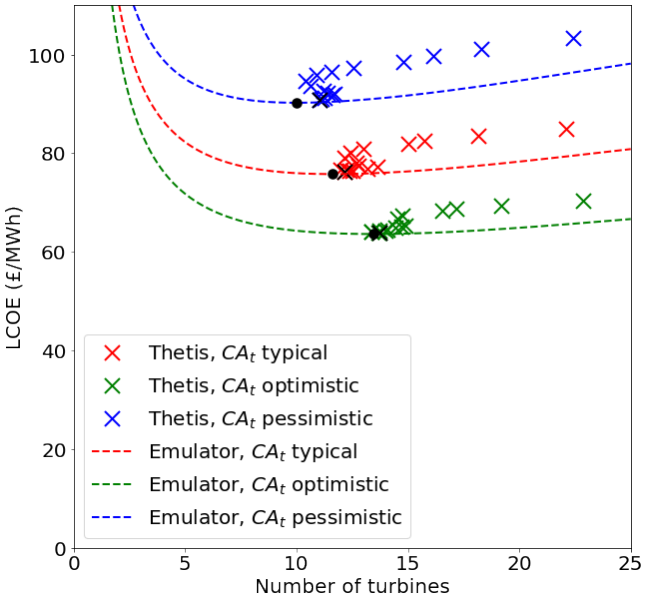

Figure 9: The emulator prediction for how LCOE varies with n_t, shown as a dashed line, compared to the final iterations of the *Thetis* optimisation, shown as coloured crosses. The optimal LCOE from the final iteration of the *Thetis* optimisation for each set of parameter values is shown as a black cross. The optimal LCOE from the emulator is marked as a black dot. The results for where CA_t is set to its max, min and typical values are shown, while all other parameters set to their typical values.

The traditional static and deterministic financial models, such as that described in Equation 8, produce a single value of LCOE or NPV for each energy project. Stochastic methods, such as Monte Carlo analysis, can capture the impact that uncertainty in the input variables has on the economic viability [53]. Monte Carlo simulations consist of repeated random sampling and statistical analysis of the results to capture sensitivities to the inputs. Monte Carlo simulations take all uncertain variables and assign a random variable to each according to an assumed distribution. In this case the uncertain variables are the inputs in Table 1 and a uniform distribution is assumed between their most pessimistic and optimistic values. The result (in this case the LCOE) is then re-calculated with the new random variables and this process is repeated many times with new random sampling each time. Ten thousand re-samplings of the LCOE within a Monte Carlo simulation ensures here that the mean and median across samples are stable each time the Monte-Carlo analysis is re-run, and is computationally practical due to the efficiency of the new emulator method. This is a novel feature of the emulator method developed in this paper, compared to other numerical methods of optimising array design which would be too computationally expensive to generate a sufficient number of samples for Monte Carlo analysis to be stable. The LCOEs found in each of the resamples can then be ordered so that the 10th, 50th (i.e. the median) and 90th percentile can be found, these are termed the P_{10}, P_{50} and P_{90} values. 90% of the resampled LCOE predictions are better (lower) than the P_{90} values, whereas only 10% of the resampled LCOE predictions are better than the P_{10} values.

This gives a much more realistic representation of how much the LCOE is likely to vary with respect to uncertainty in the inputs from Table 1. The results of such analysis are shown in Fig. 12. In practice the inputs are more likely to be distributed normally, which would result in even less variation between the P_{10} and P_{90} results. However, the standard deviation of the input errors in this paper are not known, so a more conservative uniform distribution is assumed instead.

As discussed in [21], the variability between the Optimistic, Typical and Pessimistic costs scenarios likely reflects the great rate at which costs have already fallen from the first demonstrator projects and are anticipated to fall with learning in the industry [16]. It is likely that as the cumulative installed capacity for tidal increases further the LCOE will fall from the P90 to P50 to P10 values. It is also noticeable that in the optimistic, typical and pessimistic cases, once the optimal number of turbines is exceeded, the LCOE increases, but slowly. A developer may see modest increases in LCOE as acceptable in order to produce more energy.

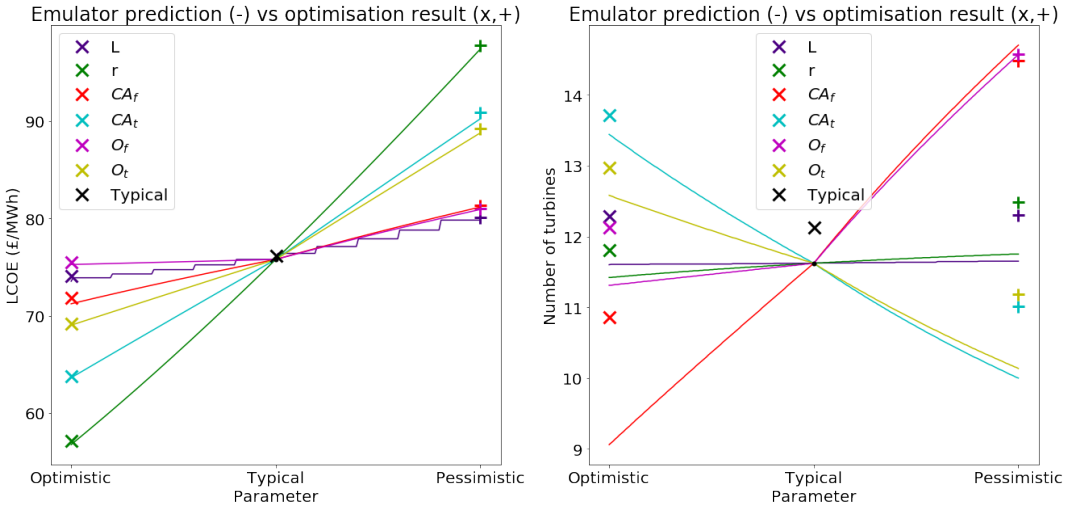

Figure 10: The impact that varying each of the input parameters, from the optimistic (x) to pessimistic (+) value given in Table 1, has on the optimal LCOE and number of turbines. This demonstrates the small errors between the optimal solution obtained through the emulator, shown as a line evaluated over all intermediate values too, and from the *Thetis* optimisation, shown as crosses. The line for L decreases in steps because the years increase discretely.

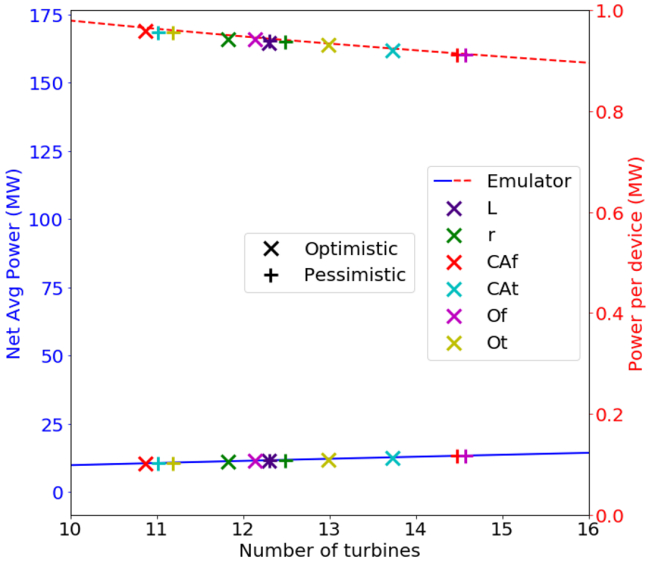

Figure 11: The net time-averaged array power and the average power per device generated in each of the optimal array designs obtained in *Thetis* as each of the input parameters are varied from their optimistic (×) to pessimistic (+) value, as given in Table 1. This demonstrates that all optimal solutions lie on the line of emulator predictions for the relationship between number of turbines and optimal power that can be achieved.

The optimal LCOE found in the pessimistic, typical and optimal scenarios are £149/MWh, £76/MWh and £37/MWh respectively. Applying Monte Carlo analysis reduced this range to a P_{90}, P_{50} and P_{10} value of £107/MWh, £83/MWh and £64/MWh respectively. The optimal number of turbines always remained between 11 and 14, highlighting that optimal array design lies between the $P_{BE} = 0.7$ and 0.8MW designs shown in Fig. 4h and 4i. In all scenarios it can be seen that increasing the number of turbines past the optimal number does not increase the LCOE dramatically. Therefore there is a lot of flexibility for developers hoping to install an array of a larger size, while keeping the LCOE below a maximal acceptable value.

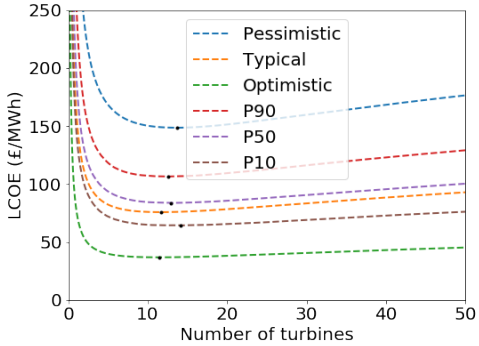

Figure 12: Predictions for the optimal LCOE that can be achieved for each number of turbines, and the resultant array design that minimises it, for the pessimistic, typical and optimistic scenarios outlines in Table 1, as well as the P_{10}, P_{50} and P_{90} values obtained through a Monte Carlo simulation assuming uniform distributions of uncertain parameters.

7 Limitations and applications

This paper presents the optimisation and in depth economic assessment of large-scale tidal arrays as well as a new method enabling rapid assessment of the LCOE for arrays of different sizes, through the use of an emulator. A number of assumptions and simplifications are made in this work to demonstrate the development of this method, without focusing on the specifics of any particular real world tidal site. This work is presented on a highly idealised domain, with very simplified tidal forcing that could be considered an approximation of an M2 tide. As such the LCOE values presented in this paper should not be taken as a prediction the cost of energy that can be achieved for tidal deployments, but instead as a demonstration of how this method can be used to predict LCOE when applied in more detail to real tidal domains.

Future work should apply this approach to the assessment of real world tidal sites with more complex bathymetry and flow. The rapid emulator method will help to increase the scope of economic analysis that can be performed without scaling up the computational expense, which will be especially important in more complex models. A more complex application of the methodology developed in this paper appears in [19]. There it is used to predict the LCOE that can be achieved in the Alderney Race as the installed capacity is increased; this demonstrates that the process works for more complex realistic sites.

The modelling approach employed here does not distinguish between the force of the rotor thrust given in Equation 12 and the drag due to the turbine structure system. A simple approach to include this, which is compatible with the depth-averaged continuous turbine modelling approach used in this paper, is presented in [42]. The total drag force is found via

$$F(\mathbf{u}) = \frac{1}{2}\rho(A_T C_t(||\mathbf{u}||) + A_{\text{support}} C_{\text{support}})||\mathbf{u}||\mathbf{u}, \tag{15}$$

where A_{support} is the cross-sectional area of the support structure and C_{support} is its drag coefficient. Various different support structure designs are available, but taking a 3m diameter monopile installation as an example, on a 16m diameter turbine with a tip to seabed clearance of 4m, the cross sectional area is $A_{support} = 3 \times (4 + 8) = 36m^2$. [42] assumed a drag coefficient for a pylon structure of $C_{support} = 0.7$, a typical value for flow past a cylinder at high Reynolds numbers. At the maximum turbine density allowed in this paper, this additional support drag term results in a dimensionless drag coefficient of 0.0039, which is small compared to the equivalent rotor drag coefficient of 0.025 (below rated for $C_T = 0.8$) but a notable increase on the standard physical bottom friction term's value of 0.0025. When applied to a real array the drag term should be updated to include the support structure of the turbine design chosen. This will result in a higher drag added by the presence of the turbines, leading to a greater impact of global blockage effects, with few turbines installed at each break even power and more significant diminishing returns as the number of turbines increases.

Another limitation and scope for further study is that this work only tests one maximum turbine density and one turbine diameter and rated power. Studies should be carried out to test the impact of varying the maximum allowable turbine density on the optimal design. This is

especially important because the wakes of each turbine are not modelled explicitly, so it may be necessary to increase the spacing requirements enforced to ensure accuracy of the depth-averaged continuous drag method [43]. Modelling the impact of changes in the turbine scale (rotor diameter and rated power) on the economics is also an important extension on this work, because it has been shown that the LCOE could reduce significantly even with small increases in turbine scale [54].

There is potential to extend this approach from continuous representation to discrete modelling of individual turbines. This would allow for the effects of accelerated bypass flow and local blockage to be investigated, which can have a substantial impact on the yield of an array [50]. The emulator based approach could substantially reduce the number of iterations needed to find the optimal number of turbines in a discrete approach, but resolving the turbines individually still requires requires a much finer mesh and is much more computationally expensive. To reduce this expense a two stage optimisation as described in [5] could be used, where the continuous optimisation provides a good initial layout, so that the discrete turbine micro-siting optimisation requires overall fewer iterations to converge. However, the emulator method would need to be validated again for testing it's accuracy at predicting the optimal power and LCOE in a discrete model.

8 Conclusions

It has been shown that an emulator can be built for rapid prediction of optimal array characteristics, with respect to many different economic models. It can be built using the results of computationally expensive adjoint optimisations over a simple functional, such as $J = P - P_{BE} \times n_t$. Only a small number of these results spread across a range of different n_t values enables us to accurately emulate a Pareto frontier between the two dominant criterion affecting the success of an array design; minimising cost, i.e. reducing n_t and maximising revenue, i.e. increasing Power generation.

The emulator that approximates this Pareto frontier has been shown to be effective at quickly evaluating a large number of functionals based on different economic metrics and different input parameters. Validation has shown this method accurately produces very similar optimal array characteristics to performing the relatively computationally expensive adjoint optimisation within *Thetis*. The fact that this emulator can accurately predict the n_t, P, LCOE and other parameters of the optimal array design very quickly enables the evaluation of the functional over a large range of input parameters and uncertainty analysis which would be unfeasibly computationally expensive otherwise. This includes the calculation of P_{10} and P_{90} confidence parameters over 10,000 Monte Carlo samples. Without building the emulator, each sample would have taken days to complete using an adjoint Thetis optimisation and Monte Carlo analysis would have been impossible. Although the underlying hydrodynamic model configuration in this paper is idealized, it should be noted that once constructed the cost of evaluating the emulator is independent of the complexity of the hydrodynamic model. Thus this approach makes it feasible to apply the same analysis to more realistic cases based on model setups with high levels of detail and accuracy.

In order to effectively test this method the LCOE was the main economic metric evaluated, however it can be applied to a vast range of other functionals including Internal Rate of Return, Payback Period and Net Present Value. The necessary economic inputs have been estimated using a review of existing literature [21], to give an estimate of how the LCOE of large-scale tidal energy arrays could be reduced with costs which fall with experience, time, economies of volume and smart array design.

Appendices

A Sensitivity with respect to LCOE inputs

A.1 Sensitivity with respect to cost estimates

Fig. 13 shows how the LCOE of the optimal array design varies as different values of CA_t, CA_f, O_t and O_f are tested in the economic (LCOE) model used for the optimisation functional. The parameters which are not being varied are set to their average values from Table 1, with the lifetime of the array set to 20 years and the discount rate set to 10%. CA_t, CA_f, O_t and O_f are all varied

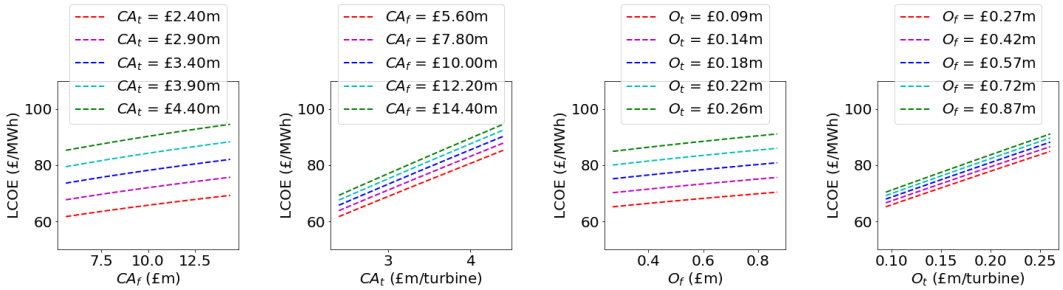

Figure 13: The optimal LCOE that can be achieved changes as each of the cost parameters are varied.

from their minimum to maximum estimates supported by the literature, from [21]. As expected, it can be seen that as each of the cost parameters is increased the optimal LCOE also increases, as energy becomes more expensive to produce.

Since Capital costs make up a higher percentage of the lifetime costs than Operational ones, especially once discounting is taken into account, varying the CAPEX parameters has more impact on the optimal LCOE than varying the OPEX parameters. This is seen despite the greater relative range of uncertainty in the OPEX parameter estimates than in the CAPEX ones. For both CAPEX and OPEX, varying the turbine-dependent component has more impact on the optimal LCOE than varying the fixed component of the costs. This is again despite the fact that the range of uncertainty in the fixed component parameter estimates is much greater than the range of uncertainty in the turbine-dependent parts. This is because although CA_f is approximately three times the size of CA_t, CA_t is multiplied by the number of turbines in an array, so it soon becomes the dominant factor as n_t increases.

Depending on the combination of input cost parameters the optimal LCOE that could be achieved varied from around £60/MWh to £100/MWh. By comparison the OREC 2018 analysis [16], predicted that tidal stream in the UK has the potential to reach an LCOE of £150/MWh at 100MW cummulative capacity and £80/MWh by 2GW cummulative capacity. While this model is of an idealised channel, it has velocities similar in magnitude to potential tidal sites such as the Alderney Race and Pentland Firth, so it seem promising that the LCOE predictions are of a similar magnitude, although slightly optimistic.

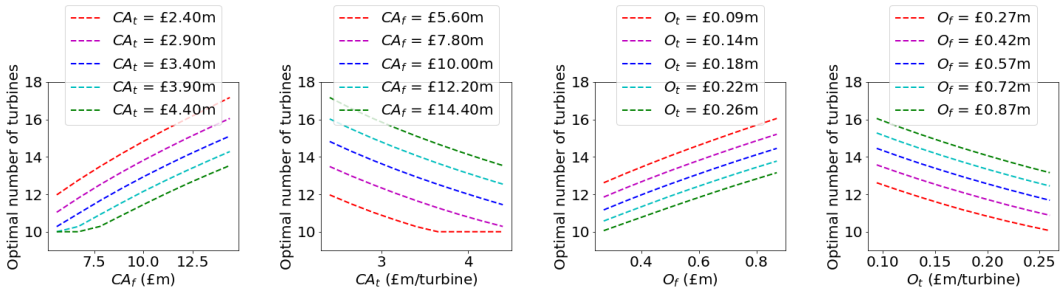

Figure 14: The number of turbines, n_t, in the array design that results in the optimal LCOE, as each of the cost parameters are varied.

Fig. 14 shows how the corresponding number of turbines in the optimal array design varies as different values of CA_t, CA_f, O_t and O_f are considered. Predictably, as the turbine-dependent costs are increased the optimal number of turbines decreases, since they are more expensive to install. However, as the fixed costs increase the optimal number of turbines increases. As CA_f becomes larger with respect to CA_t, the impact of economies of volume becomes more significant and more turbines are required to spread the initial fixed costs over. Similarly, the optimal n_t

increases as O_f increases with respect to O_t. Again, the uncertainty in OPEX estimates have less impact on the optimal number of turbines than the uncertainty in CAPEX estimates. This is despite there being greater variation in OPEX, due to CAPEX being a higher factor in the lifetime discounted costs of an array. However, the optimal number of turbines varies by a similar very amount over the minimum to maximum range of fixed costs compared to turbine-dependent costs, despite the LCOE being more sensitive to variation in turbine-dependent costs.

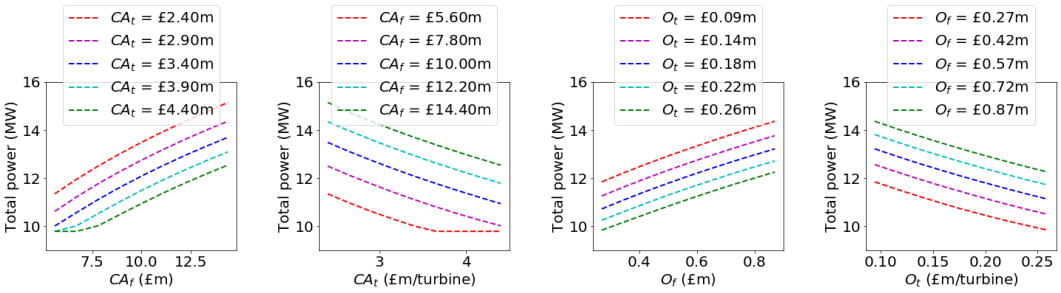

Figure 15: The total array power of the design that results in the optimal LCOE as the cost parameters are varied.

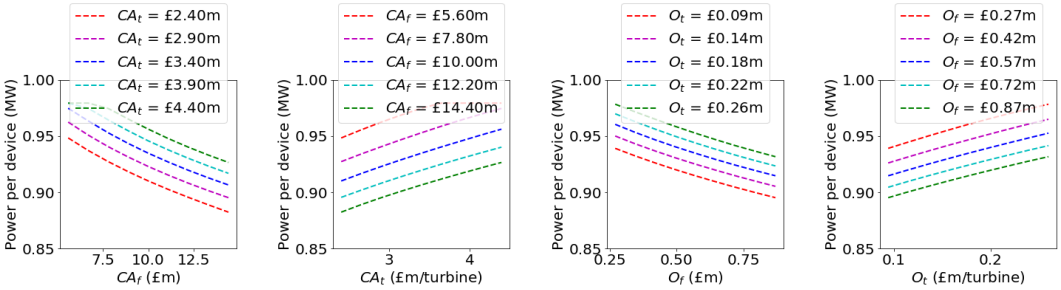

Figure 16: The average power per device in design that results in the optimal LCOE as the cost parameters are varied.

Fig. 15 and Fig. 16 show how the total array power and the average power per device of the optimal array designs vary with different values of CA_t, CA_f, O_t and O_f, respectively. They show that as the fixed costs increase (for both CAPEX and OPEX), the total array power increases, but the average power per device decreases. This corresponds to the increase in the number of turbines with increased fixed costs shown in Fig. 14. The higher the fixed costs the more power needs to be generated to compensate for it, even if this comes at the expense of more turbines and a lower return per turbine. Conversely, as the turbine-dependent costs increase the total power decreases but the average power per device increases. As the turbines become the more costly part of the array expenses, fewer turbines should be installed, allowing a higher percentage of them to fit in the fastest flowing locations. Similarly to LCOE and n_t, varying the CAPEX has a greater impact on the total array power and average power per device than varying the OPEX.

A.2 Sensitivity with respect to array lifetime and discount rate

Similarly, the sensitivity of the optimal design to change in L and r with respect to one another can be investigated. Fig. 17 shows how varying both parameters impacts the optimal LCOE and the number of turbines at which the optimal LCOE is found. Varying the discount rate has a bigger impact on the optimal LCOE than varying the lifetime of the array and as the discount rate increases the impact of the lifetime on both the LCOE and the number of turbines decreases. This is because discounting minimises the impact of the revenue and expenditure in the final years

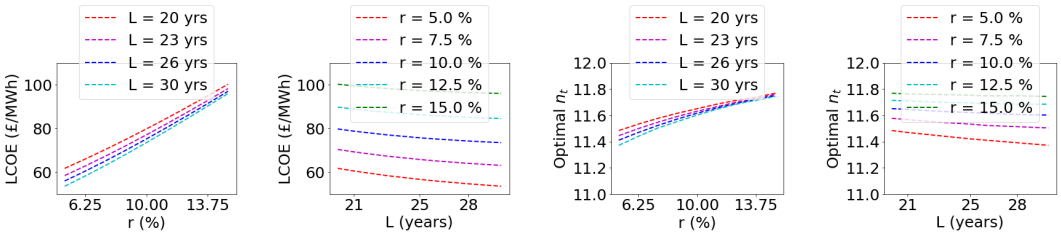

Figure 17: The total LCOE and number of turbines in the array design that results in the optimal LCOE as the lifetime of the array, L, and the discount rate, r, are varied.

of the array on the LCOE and the greater the discount rate the less impact increasing the lifetime will have.

While lifetime has relatively little impact on the LCOE, the discount rate has an impact of similar magnitude to varying the cost inputs, shown in Fig. 13. However both the discount rate and the lifetime of the array have very little impact on the optimal number of turbines, compared to the costs shown in Fig. 14. This is because the balance of fixed to turbine-dependent costs changes the extent to which there are economies of volume, and therefore moves the optimal number of turbines more, whereas L and r shift the LCOE vs n_t curve (such as that shown in Fig. 8) up and down, but do not change its shape much.

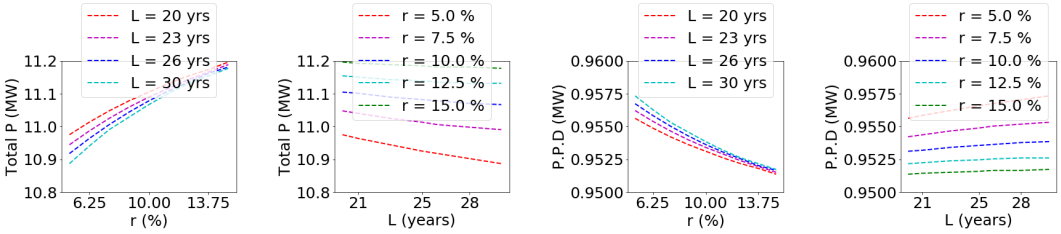

Figure 18: The total array power and the average power per device in the design that results in the optimal LCOE as the lifetime of the array, L, and the discount rate, r, are varied.

Fig. 18 shows how the total array power and the average power per device of the optimal array designs vary with different values of L and r. Again it can be seen that the discount rate has more impact than the lifetime on the total and average power generation, but both have much less impact than varying CA_t, CA_f, O_t and O_f, as shown in Fig. 15 and Fig. 16. Since varying these parameters has very little impact on the number of turbines, it is not changing the array design, and therefore the power generated by much, it is just changing the profitability (and therefore LCOE) of the array. Throughout the whole range of L and r values found in Table 1, the optimal number of turbines remains between 11 and 12, corresponding to the array design shown in Fig. 4i and thus the power generated remains roughly the same.

9 Acknowledgements

ZLG acknowledges the support of Engineering and Physical Sciences Research Council (EPSRC) Centre for Doctoral Training in the Mathematics of Planet Earth [grant number EP/L016613/1].

DSC acknowledges the financial support of the Tidal Stream Industry Energiser project (TIGER), co-financed by the European Regional Development Fund through the Interreg France (Channel) England Programme.

SCK and MDP would like to acknowledge the support of the UK's Engineering and Physical Sciences Research Council (EPSRC) [grant numbers EP/M011054/1, EP/L000407/1 and EP/R029423/1].

All authors would like to thank the Imperial College London Research Computing Service for their support.

References

[1] "Contracts for Difference Allocation Round 3 Results," Tech. Rep., 2019. [Online]. Available: https://www.gov.uk/government/publications/contracts-for-difference-cfd-allocation-round-3-results

[2] S. Astariz and G. Iglesias, "The economics of wave energy: A review," 2015. [Online]. Available: https://www.sciencedirect.com/science/article/pii/S1364032115000714

[3] T. Stallard, R. Collings, T. Feng, and J. Whelan, "Interactions between tidal turbine wakes: experimental study of a group of three-bladed rotors," *Phil. Trans. R. Soc. A.*, vol. 371, no. 20120159, 2013. [Online]. Available: http://dx.doi.org/10.1098/rsta.2012.0159http://rsta.royalsocietypublishing.org.

[4] P. Mycek, B. Gaurier, G. Germain, G. Pinon, and E. Rivoalen, "Experimental study of the turbulence intensity effects on marine current turbines behaviour. Part II: Two interacting turbines," *Renewable Energy*, vol. 68, pp. 876–892, 8 2014.

[5] S. W. Funke, S. C. Kramer, and M. D. Piggott, "Design optimisation and resource assessment for tidal-stream renewable energy farms using a new continuous turbine approach," *Renewable Energy*, vol. 99, pp. 1046–1061, 2016. [Online]. Available: doi:10.1016/j.renene.2016.07.039

[6] S. W. Funke, P. E. Farrell, and M. D. Piggott, "Tidal turbine array optimisation using the adjoint approach," *Renewable Energy*, vol. 63, pp. 658–673, 3 2014. [Online]. Available: doi:10.1016/j.renene.2013.09.031

[7] D. M. Culley, S. W. Funke, S. C. Kramer, and M. D. Piggott, "Integration of cost modelling within the micro-siting design optimisation of tidal turbine arrays," *Renewable Energy*, vol. 85, pp. 215–227, 2016. [Online]. Available: doi:10.1016/j.renene.2015.06.013

[8] R. J. du Feu, S. W. Funke, S. C. Kramer, D. M. Culley, J. Hill, B. S. Halpern, and M. D. Piggott, "The trade-off between tidal-turbine array yield and impact on flow: A multi-objective optimisation problem," *Renewable Energy*, vol. 114, pp. 1247–1257, 12 2017. [Online]. Available: doi:10.1016/j.renene.2017.07.081

[9] P. Stansby and T. Stallard, "Fast optimisation of tidal stream turbine positions for power generation in small arrays with low blockage based on superposition of self-similar far-wake velocity deficit profiles," *Renewable Energy*, 2016.

[10] D. S. Coles and T. Walsh, "Mechanisms for reducing the cost of tidal stream energy," in *13th European Wave and Tidal Energy Conference*, Naples, 2019, pp. 1836–1–8.

[11] S. C. Kramer and M. D. Piggott, "A correction to the enhanced bottom drag parameterisation of tidal turbines," *Renewable Energy*, vol. 92, pp. 385–396, 2016. [Online]. Available: doi:10.1016/j.renene.2016.02.022

[12] T. Kärnä, S. C. Kramer, L. Mitchell, D. A. Ham, M. D. Piggott, and A. M. Baptista, "Thetis coastal ocean model: discontinuous Galerkin discretization for the three-dimensional hydrostatic equations," *Geosci. Model Dev*, vol. 11, pp. 4359–4382, 2018. [Online]. Available: https://doi.org/10.5194/gmd-11-4359-2018

[13] R. J. du Feu, S. W. Funke, S. C. Kramer, J. Hill, and M. D. Piggott, "The trade-off between tidal-turbine array yield and environmental impact: A habitat suitability modelling approach," *Renewable Energy*, vol. 143, pp. 390–403, 12 2019. [Online]. Available: doi:10.1016/j.renene.2019.04.141

[14] Z. L. Goss, S. C. Kramer, A. Avdis, C. J. Cotter, and M. D. Piggott, "Variations in the optimal design of a tidal stream turbine array with costs," in *Oxford Tidal Energy Workshop*, Oxford, 2019, pp. 33–34. [Online]. Available: http://www2.eng.ox.ac.uk/tidal/ote2019-1/proceedings-ote2019

[15] Z. L. Goss, S. C. Kramer, A. Avdis, C. J. Cotter, and M. Piggott, "Economic optimisation of large scale tidal stream turbine arrays," in *13th European Wave and Tidal Energy Conference*, Naples, 2019, pp. 1598–1–8.

[16] G. Smart and M. Noonan, "Tidal stream and wave energy cost reduction and industrial benefit," *Catapult ORE*, 2018. [Online]. Available: https://www.marineenergywales.co.uk/wp-content/uploads/2018/05/ORE-Catapult-Tidal-Stream-and-Wave-Energy-Cost-Reduction-and-Ind-Benefit-FINAL-v03.02.pdf

[17] C. D. R. Donovan and C. Corbishley, "The cost of capital and how it affects climate change mitigation investment," *Grantham Institute*, no. 15, 2016. [Online]. Available: https://www.imperial.ac.uk/media/imperial-college/grantham-institute/public/publications/briefing-papers/the-cost-of-capital-and-how-it-affects-climate-change-mitigation-investment-v2-Grantham-BP-15.pdf

[18] S. A. Morse, "The Green Investment Bank," 2017. [Online]. Available: https://www.nao.org.uk/report/the-green-investment-bank/

[19] Z. L. Goss, D. S. Coles, and M. D. Piggott, "Identifying economically viable tidal sites within the Alderney Race through optimization of levelized cost of energy," *Philosophical Transactions of the Royal Society A: Mathematical, Physical and Engineering Sciences*, vol. 378, no. 2178, p. 20190500, 8 2020. [Online]. Available: doi:10.1098/rsta.2019.0500

[20] "Lessons Learnt from MeyGen Phase 1A Part 2/3: Construction Phase," 2018. [Online]. Available: https://ore.catapult.org.uk/lessons-learnt-from-meygen-phase-1a-part-2-of-3-design-phase/

[21] Z. L. Goss, D. S. Coles, and M. D. Piggott, "Economic analysis of tidal stream turbine arrays: a review," 2021. [Online]. Available: https://we.need.to.upload.this.to.spiral.pdf

[22] "Lessons Learnt from MeyGen Phase 1a Part 1/3: Design Phase," 2017. [Online]. Available: https://tethys.pnnl.gov/sites/default/files/publications/MeyGen-2017-Part1.pdf

[23] J. Thiébot, S. Guillou, and E. Droniou, "Influence of the 18.6-year lunar nodal cycle on the tidal resource of the Alderney Race, France," *Applied Ocean Research*, vol. 97, p. 102107, 4 2020. [Online]. Available: doi:10.1016/j.apor.2020.102107

[24] I. D. Haigh, M. Eliot, and C. Pattiaratchi, "Global influences of the 18.61 year nodal cycle and 8.85 year cycle of lunar perigee on high tidal levels," *Journal of Geophysical Research: Oceans*, vol. 116, no. 6, 6 2011. [Online]. Available: doi:10.1029/2010JC006645

[25] S. Faulstich, B. Hahn, and P. J. Tavner, "Wind turbine downtime and its importance for offshore deployment," *Wind Energy*, vol. 14, no. 3, pp. 327–337, 4 2011. [Online]. Available: doi:wiley.com/10.1002/we.421

[26] L. Ziegler, E. Gonzalez, T. Rubert, U. Smolka, and J. J. Melero, "Lifetime extension of onshore wind turbines: A review covering Germany, Spain, Denmark, and the UK," *Renewable and Sustainable Energy Reviews*, vol. 82, pp. 1261–1271, 2 2018. [Online]. Available: doi:10.1016/j.rser.2017.09.100

[27] S. P. Neill, J. R. Jordan, and S. J. Couch, "Impact of tidal energy converter (TEC) arrays on the dynamics of headland sand banks," *Renewable Energy*, vol. 37, no. 1, pp. 387–397, 1 2012.

[28] A. Vazquez and G. Iglesias, "Capital costs in tidal stream energy projects – A spatial approach," *Energy*, vol. 107, pp. 215–226, 7 2016. [Online]. Available: doi:10.1016/j.energy.2016.03.123

[29] "Lessons Learnt from MeyGen Phase 1A: Final Summary Report," 2020. [Online]. Available: https://bit.ly/2BffaOD

[30] P. Higgins and A. M. Foley, "Review of offshore wind power development in the United Kingdom," in *2013 12th International Conference on Environment and Electrical Engineering*. IEEE, 5 2013, pp. 589–593. [Online]. Available: doi:10.1109/EEEIC.2013.6549584

[31] "International LCOE for Ocean Energy Technology," 2015. [Online]. Available: https://www.ocean-energy-systems.org/news/international-lcoe-for-ocean-energy-technology/

[32] "Bluemull Sound." [Online]. Available: https://www.novainnovation.com/bluemull-sound

[33] "SIMEC Atlantis Energy Unveils World's Largest Single Rotor Tidal Turbine, the AR2000 | SIMEC Atlantis Energy." [Online]. Available: https://simecatlantis.com/2018/09/13/simec-atlantis-energy-unveils-worlds-largest-single-rotor-tidal-turbine-the-ar2000/

[34] A. S. Bahaj, A. F. Molland, J. R. Chaplin, and W. M. J. Batten, "Power and thrust measurements of marine current turbines under various hydrodynamic flow conditions in a cavitation tunnel and a towing tank," *Renewable Energy*, vol. 32, no. 3, pp. 407–426, 3 2007. [Online]. Available: doi:10.1016/j.renene.2006.01.012

[35] S. Draper, "Tidal Stream Energy Extraction in Coastal Basins," Ph.D. dissertation, St Catherine's College, Oxford, 2011. [Online]. Available: http://www2.eng.ox.ac.uk/civil/publications/theses/draper.pdf

[36] J. Thiébot, D. S. Coles, A.-C. Bennis, N. Guillou, S. Neill, S. Guillou, and M. Piggott, "Numerical modelling of hydrodynamics and tidal energy extraction in the Alderney Race: a review," *Philosophical Transactions of the Royal Society A: Mathematical, Physical and Engineering Sciences*, vol. 378, no. 2178, p. 20190498, 8 2020. [Online]. Available: doi:10.1098/rsta.2019.0498

[37] D. S. Coles, L. S. Blunden, and A. S. Bahaj, "Assessment of the energy extraction potential at tidal sites around the Channel Islands," *Energy*, vol. 124, pp. 171–186, 2017. [Online]. Available: doi:10.1016/j.energy.2017.02.023

[38] A. Pérez-Ortiz, A. G. Borthwick, J. McNaughton, H. C. Smith, and Q. Xiao, "Resource characterization of sites in the vicinity of an island near a landmass," *Renewable Energy*, vol. 103, pp. 265–276, 4 2017. [Online]. Available: doi:10.1016/j.renene.2016.10.086

[39] A. S. Iyer, S. J. Couch, G. P. Harrison, and A. R. Wallace, "Variability and phasing of tidal current energy around the United Kingdom," *Renewable Energy*, vol. 51, pp. 343–357, 3 2013.

[40] M. Lewis, S. P. Neill, P. E. Robins, and M. R. Hashemi, "Resource assessment for future generations of tidal-stream energy arrays," *Energy*, vol. 83, pp. 403–415, 4 2015.

[41] F. Rathgeber, D. A. Ham, L. Mitchell, M. Lange, F. Luporini, A. T. T. Mcrae, G.-T. Bercea, G. R. Markall, P. H. J. Kelly, . D. A. Ham, and . P. H. J. Kelly, "Firedrake: Automating the finite element method by composing abstractions," *ACM Transactions on Mathematical Software*, vol. 43, no. 3, p. 24, 2016. [Online]. Available: http://dx.doi.org/10.1145/2998441

[42] R. Martin-Short, J. Hill, S. C. Kramer, A. Avdis, P. A. Allison, and M. D. Piggott, "Tidal resource extraction in the Pentland Firth, UK: Potential impacts on flow regime and sediment transport in the Inner Sound of Stroma," *Renewable Energy*, vol. 76, pp. 596–607, 4 2015.

[43] D. S. Coles, L. S. Blunden, and A. S. Bahaj, "Experimental validation of the distributed drag method for simulating large marine current turbine arrays using porous fences," *International Journal of Marine Energy*, 2016.

[44] D. Coles, C. Greenwood, A. Vogler, T. Walsh, and D. Taaffe, "Assessment of the turbulent flow upstream of the Meygen Phase 1A tidal stream turbines," AWTEC, Tech. Rep., 2018.

[45] T. Blackmore, W. M. J. Batten, and A. S. Bahaj, "Influence of turbulence on the wake of a marine current turbine simulator," *Proc. R. Soc. A*, vol. 470, 2014. [Online]. Available: http://dx.doi.org/10.1098/rspa.2014.0331

[46] C. R. Vogel, R. H. Willden, and G. T. Houlsby, "Power available from a depth-averaged simulation of a tidal turbine array," *Renewable Energy*, vol. 114, pp. 513–524, 12 2017.

[47] A. J. Goward Brown, S. . Neill, and M. . Lewis, "Tidal energy extraction in three-dimensional ocean models," *Renewable Energy*, vol. 114, pp. 244–257, 2017. [Online]. Available: https://doi.org/10.1016/j.renene.2017.04.032

[48] S. Waldman, S. Yamaguchi, R. O'Hara Murray, and D. Woolf, "Tidal resource and interactions between multiple channels in the Goto Islands, Japan," *International Journal of Marine Energy*, vol. 19, pp. 332–344, 9 2017.

[49] European Marine Energy Centre Ltd, "Assessment of Tidal Energy Resource," EMEC, Tech. Rep., 2009. [Online]. Available: http://www.emec.org.uk/assessment-of-tidal-energy-resource/

[50] C. A. Consul, R. H. Willden, and S. C. McIntosh, "Blockage effects on the hydrodynamic performance of a marine cross-flow turbine," *Philosophical Transactions of the Royal Society A: Mathematical, Physical and Engineering Sciences*, vol. 371, no. 1985, 2 2013.

[51] Z. L. Goss, M. D. Piggott, S. C. Kramer, A. Avdis, A. Angeloudis, and C. J. Cotter, "Competition effects between nearby tidal turbine arrays-optimal design for Alderney Race," in *3rd International Conference on Renewable Energies Offshore*, Lisbon, 2018, pp. 255–262.

[52] T. Divett, R. Vennell, and C. Stevens, "Optimization of multiple turbine arrays in a channel with tidally reversing flow by numerical modelling with adaptive mesh," *Philosophical Transactions of the Royal Society A: Mathematical, Physical and Engineering Sciences*, vol. 371, no. 1985, p. 20120251, 2 2013. [Online]. Available: https://royalsocietypublishing.org/doi/10.1098/rsta.2012.0251

[53] S. Raychaudhuri, "Introduction to monte carlo simulation," in *Proceedings - Winter Simulation Conference*, 2008, pp. 91–100.

[54] D. S. Coles and T. Walsh, "Mechanisms for reducing the cost of tidal stream energy," in *13th European Wave and Tidal Energy Conference*, Naples, 2019, pp. 1836–1.

Nomenclature	
Acronyms	
CAPEX	Capital Expenditure
OPEX	Operational Expenditure
NPV	Net Present Value
IRR	Internal rate of return
ROI	Return on investment
PP	Payback period
LCOE	Levelised cost of energy
OREC	Offshore Renewable Energy Catapult
CCFI	Centre for Climate Finance Institute
GIB	Green Investment Bank
UFL	Unified Form Language
ADCP	Acoustic Doppler current profiler
P10	10th percentile in probabilistic Monte Carlo resampling
P50	50th percentile (the median) in probabilistic Monte Carlo resampling
P90	90th percentile in probabilistic Monte Carlo resampling
Symbols	
CA_t	Turbine-dependent CAPEX (per year)
O_t	Turbine-dependent OPEX (per year)
CA_f	Fixed CAPEX (per year)
O_f	Fixed OPEX (per year)
r	Discount rate
L	Lifetime of array
Rev_i	Revenue in year i
Ex_i	Total expenditure in year i
n_t	Number of turbines
P_{avg}	Average array power
P_{BE}	Break even power (per turbine)
t_i	Number of hours generating in year i
T_e	Electricity tariff
C_T	Thrust Coefficient
C_P	Power Coefficient
A_T	Swept area of turbine rotor
$C_{support}$	Drag coefficient of turbine support structure
$A_{support}$	Cross-sectional area of turbine support structure
J	Optimisation functional
EV	Economies of volume rate
η	Free surface perturbation
t	Time
H	Total water depth
$\mathbf{u}$	2D depth averaged velocity vector
ν	Kinematic viscosity
C_d	Dimensionless drag coefficient
L_d	length of domain
B_d	Width of domain
$_i$	Island diameter
s	Minimum distance from island to southern landmass
A_f	Farm area
L_f	Farm length
B_f	Farm width
h_0	Depth in main part of domain
a	Amplitude of free surface perturbation
ω_t	Frequency of free-surface perturbation
$d(\mathbf{x})$	Spatially varying turbine density field
c_t	Turbine bottom friction coefficient
u_{rated}	Rated speed

Table 1: Estimates for the parameters used in the economic models, and the amount they vary. Taken from [21].

Symbol	Description	Value range			Units
		Optimistic	Typical	Pessimistic	
CA_f	Fixed CAPEX	5.6	9.2	14.4	£m
CA_t	Turbine-dependant CAPEX	2.4	3.3	4.4	£m/turbine
O_f	Fixed OPEX	0.27	0.32	0.87	£m/year
O_t	Turbine-dependant OPEX	0.094	0.15	0.26	£m/year/turbine
r	Discount rate	0.05	0.10	0.15	N/A
L	Lifetime of an array	30	25	20	years